



INDC(NDS)-0767
Distr. IBA,NM,G

INDC International Nuclear Data Committee

R-Matrix Codes for Charged-particle Reactions in the Resolved Resonance Region (4)

Summary Report of the Consultants' Meeting,
IAEA Headquarters, Vienna, Austria
27-29 August 2018

Prepared by

Helmut Leeb
Technische Universität Wien
Vienna, Austria

Paraskevi Dimitriou
IAEA, Vienna, Austria

Ian Thompson
Lawrence Livermore National Laboratory
Livermore CA, USA

November 2018

Selected INDC documents may be downloaded in electronic form
from <http://nds.iaea.org/publications>
or sent as an e-mail attachment.

Requests for hardcopy or e-mail transmittal should be directed to
NDS.Contact-Point@iaea.org

or to:

Nuclear Data Section
International Atomic Energy Agency
Vienna International Centre
PO Box 100
1400 Vienna
Austria

Printed by the IAEA in Austria

November 2018

R-Matrix Codes for Charged-particle Reactions in the Resolved Resonance Region (4)

Summary Report of the Consultants' Meeting,
IAEA Headquarters, Vienna, Austria
27-29 August 2018

Prepared by

Helmut Leeb
Technische Universität Wien
Vienna, Austria

Paraskevi Dimitriou
IAEA, Vienna, Austria

Ian Thompson
Lawrence Livermore National Laboratory
Livermore CA, USA

ABSTRACT

A Consultants' Meeting was held at the IAEA Headquarters from 27 to 29 August 2018, to discuss the results of a coordinated effort to verify R-matrix codes through a well-defined exercise. Six R-matrix codes were included in this verification exercise: AMUR, AZURE2, EDA, RAC, SFRESCOX, and SAMMY. Furthermore, the contents of the final publication of this exercise were considered in this meeting. This report summarizes the presentations and technical discussions of the meeting, as well as any additional actions that were proposed.

November 2018

Contents

1. Introduction	7
2. Test 1a	7
2.1. Summary of results, James De Boer, Univ. Notre-Dame	8
2.2. Discussion.....	13
3. Test 1b.....	14
3.1. Test 1b results.....	14
3.1.1. Test 1b results with SFRESCOX , I.J. Thompson, LLNL.....	14
3.1.2. Test 1b results with AZURE, R.J. DeBoer, Univ. Notre Dame.....	21
3.1.3. Test 1b results with AMUR, S. Kunieda, JAEA	25
3.1.4. Test 1b results with RAC, Z. Chen, Tsinghua University of Beijing	27
3.1.5. Test 1b results with SAMMY, M. Pigni, ORNL	39
3.1.6. ⁷ Be analysis with EDA, G. Hale, LANL	48
3.2. Discussion of Test 1b.....	49
4. Test 2.....	51
5. Test 3.....	51
6. Conclusions and Recommendations	52
7. List of Actions	53
Annex 1: Preliminary Agenda.....	55
Annex 2: List of Participants.....	57
Annex 3: Links to Presentations.....	59

1. Introduction

The IAEA Nuclear Data Section is coordinating an international effort to (i) compare and verify existing R-matrix codes on charged-particle reactions in the resolved resonance region, (ii) produce evaluations of charged-particle cross sections for applications and finally (iii) disseminate the evaluated data through general and special purpose nuclear data libraries.

The kick-off meeting of this coordinated project was held on 7-9 December 2015 at the IAEA in Vienna. The focus of the first meeting was the specific capabilities of the existing R-matrix codes and the translatability of R-matrix calculations produced by the various codes. A summary report of the meeting is published as INDC(NDS)-0703 (<https://www-nds.iaea.org/publications/indc/indc-nds-0703/>).

In the two subsequent meetings held on 5-7 December 2016 and 28 to 30 June 2017 at the IAEA in Vienna, the working group met to discuss the details and results of a common exercise that was carried out in two parts: the first part aimed at comparing the R-matrix algorithms implemented in the codes (Test 1a), while the second part compared the minimization techniques and fitting procedures applied by the evaluators (Test 1b). The exercises involved fitting the two channels ${}^3\text{He}+{}^4\text{He}$ and $p+{}^6\text{Li}$ forming the ${}^7\text{Be}$ compound system at sufficiently low excitation energies to exclude other reaction channels. The details of the exercise and results, as well as additional systematic comparisons that resulted from the technical discussions can be found in the summary reports of the meetings, INDC(NDS)-0726 (<https://www-nds.iaea.org/publications/indc/indc-nds-0726/>) and INDC(NDS)-0737 (<https://www-nds.iaea.org/publications/indc/indc-nds-0737/>), respectively.

The fourth meeting was held from 27 to 29 August 2018 with the purpose of reviewing the final conclusions of part one (Test 1a) and comparing the results of the second part (Test 1b). Five codes were involved in the exercise: AMUR, AZURE2, RAC, SFRESCOX and SAMMY. Results from the EDA code were also presented and will be included in the final publication.

Seven participants from four countries attended the meeting: Z. Chen (People's Rep. of China), R.J. Deboer (USA), S. Kunieda (Japan), H. Leeb (Austria), M. Pigni (USA), T. Srdinko (Austria), I.J. Thompson (USA), G. Hale (USA), P. Archier (France) and S. Kopecky (EC), including IAEA staff P. Dimitriou (Scientific Secretary) and A. Trkov.

The participants were welcomed to the IAEA by the Nuclear Data Section Head, Arjan Koning. P. Dimitriou briefly introduced the objective and scope of the meeting. I. Thompson was appointed Chairman and H. Leeb rapporteur. After the Agenda was adopted, the meeting continued with participants' presentations according to the Agenda. The meeting agenda and participants' coordinates can be found in Annexes 1 and 2, respectively, while the links to the presentations are given in Annex 3.

2. Test 1a

The purpose of Test 1a was to verify that all the codes obtain the same results when using standard R-matrix theory to calculate cross sections for charged-particle reactions leading to the compound system ${}^7\text{Be}$. A set of initial conditions was agreed on and was adopted by all the code developers. These initial conditions are described in detail in [INDC\(NDS\)-0737](#) (Appendix). In the following sections we discuss the results of Test 1a.

2.1. Summary of results, James De Boer, Univ. Notre-Dame

Initial calculations showed large differences in the cross sections between the calculations made by the participants. Many of these differences came from simple typos in input files and misinterpretation of the meaning of some of the parameters. However, several errors or approximations were also discovered in the different codes and most of these issues were resolved. The following tables indicate issues, and possible solutions, encountered by the different participants.

- James deBoer (AZURE2)
 - Found several small typos in the energies and reduced widths entered into the calculation.
 - Used exact masses instead of integer mass to calculate the channel radii.
- Ian Thompson (SFRESCOX)
 - Put Huby phases into the transformation between SFRESCOX amplitudes and other amplitudes
 - Poor switching of incoming channels
 - $dW/dr = k dW/d\rho$ (factor is k , not k^2)
- Marco Pigni (SAMMY-Modified)
 - Updated the Coulomb functions resulting in the ability to calculate the shift function at subthreshold energies. S -matrix algorithm was updated to account for subthreshold effects.
- Satoshi Kawano (AMUR)
- Zhenpeng Chen (RAC)
- Vivian Dimitriou (SAMMY-Public): the differences observed between SAMMY-Public and SAMMY-Modified essentially reflect the impact of the changes implemented in the latter code.

Table 2.1 below indicates the level of consistency obtained between the different calculations. The level of consistency was quantified by taking the ratios of cross sections and where numerical values are cited referring to the level of consistency this is what is being compared. The highest level of consistency was obtained between the calculations of AZURE2 and SFRESCOX. The codes were found to agree in all calculations to better than 1×10^{-4} . This was certainly not the case to begin with and many iterations of comparisons and updated calculations were required to get to this level. Several approximations were also known to exist in SAMMY related to parameter transformations. These approximations were replaced by their exact implementations and the level of agreement improved between SAMMY, AZURE2 and SFRESCOX to better than 1×10^{-3} for all calculations. Finally, calculations with AMUR and RAC were never able to achieve these levels of consistency. A level of 1×10^{-2} agreement was obtained compared to the (p,p) and (p, α) data, but large discrepancies of up to 10's of percent were observed in the high energy alpha scattering data. Comparisons are shown in Figs. (2.1-2.4).

TABLE 2.1. Level of constancy, given by the ratio of the cross sections relative to the calculations of AZURE2, observed by taking ratios of the cross sections calculated by the different participants using different R-matrix codes.

Data set	AMUR	SAMMY	SFRESCOX	RAC
Barnard1964629	10^{-1}	10^{-2}	10^{-4}	>1
{PhysRev.130.2034	10^{-2}	10^{-4}	10^{-4}	10^{-2}
PhysRevC.20.1984	10^{-2}	10^{-3}	10^{-5}	10^{-2}
PhysRev.163.964	10^{-1}	10^{-3}	10^{-4}	>1

The largest discrepancy between the different calculations was observed in those using the Spiger and Tombrello [2.4] energies and angles, the highest energies for the alpha scattering. Since the difference between the different calculations was so large, four different plots are shown with the ratio axis adjusted to 1%, 5%, 10%, and 20% in Figs. (2.4-2.7), respectively.

Calculations will continue in order to resolve the inconsistencies between the calculations of the different codes. The future goal ideally is to achieve a level of agreement of 1×10^{-3} , but a level of 5×10^{-3} has also been deemed to be acceptable.

References

- [2.1] A.C.L. Barnard and C.M. Jones and G.C. Phillips, Nucl. Physics **50**, 629 - 640 (1964).
- [2.2] A.J. Elwyn, R.E. Holland, C.N. Davids, L. Meyer-Schützmeister, F.P. Mooring, and W. Ray, Phys. Rev. C **20**, 1984-1992 (1979).
- [2.3] J.A. McCray, Phys. Rev. **130**, 2034-2042 (1963).
- [2.4] R.J. Spiger and T.A. Tombrello, Phys. Rev. **163**, 964-984 (1967).

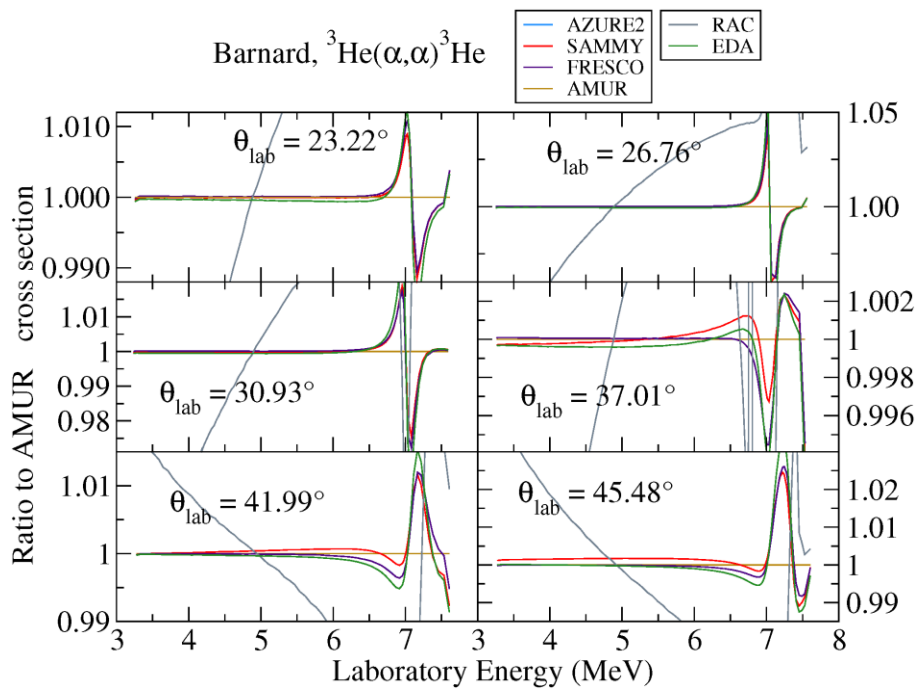


FIG. 2.1. De Boer: Comparison of calculations for the ${}^3\text{He}(\alpha, \alpha){}^3\text{He}$ reaction using the energies and angles of the Barnard data [2.1]. Ratios are with respect to the AMUR code.

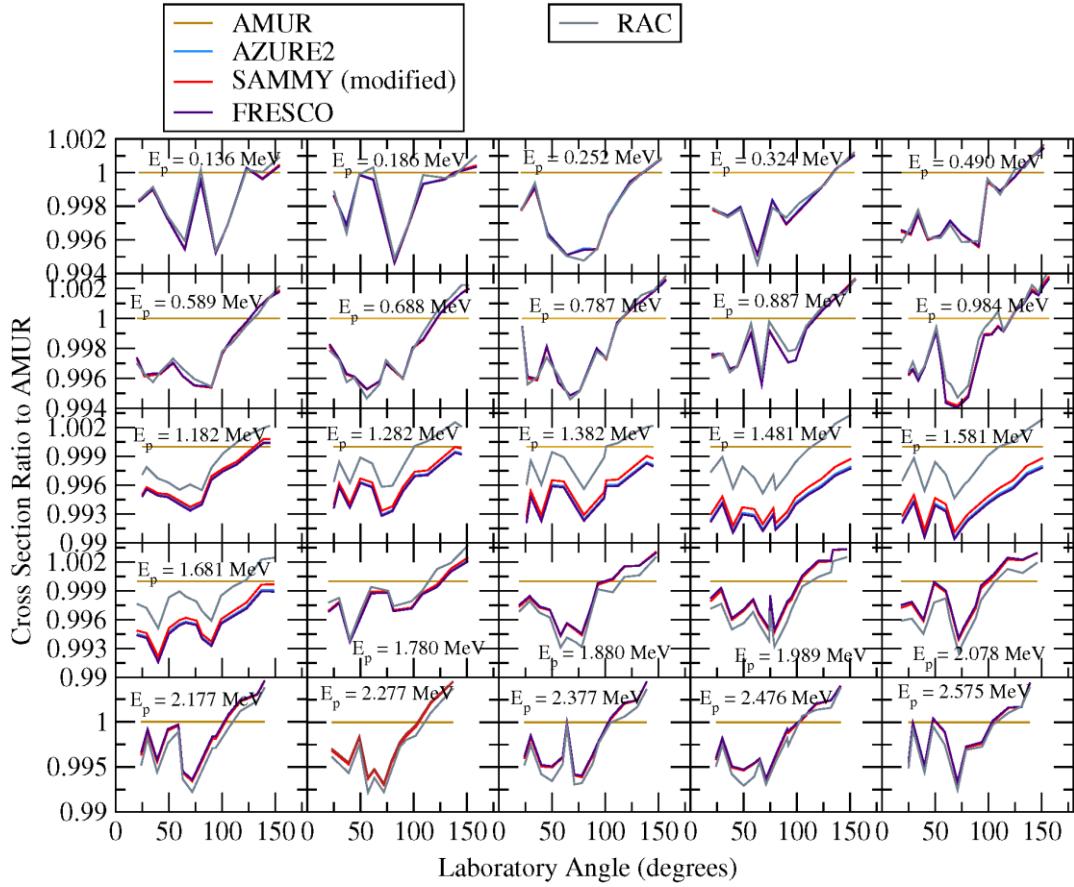


FIG. 2.2. De Boer: Comparison of calculations for the ${}^6\text{Li}(p,\alpha){}^3\text{He}$ reaction using the energies and angles of the Elwyn data [2.2]. Ratios are with respect to the AMUR2 code.

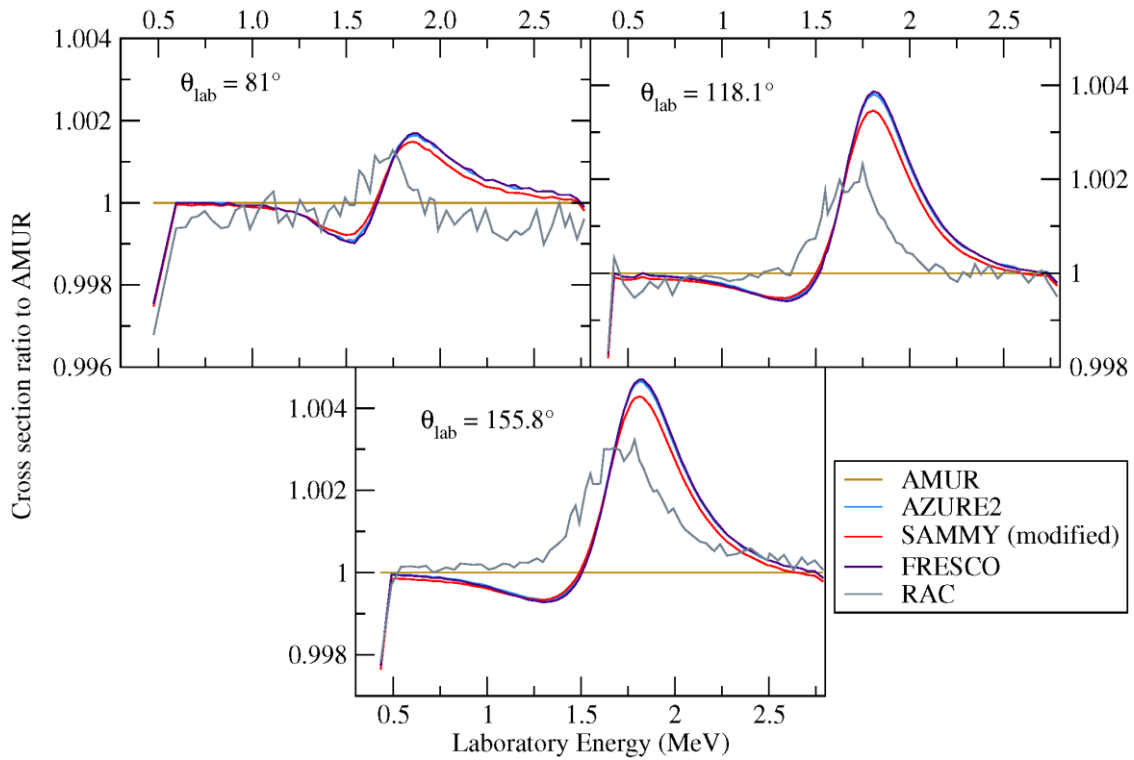


FIG. 2.3. De Boer: Comparison of calculations for the ${}^6\text{Li}(p,p){}^6\text{Li}$ reaction using the energies and angles of the McCray data [2.3]. Ratios are with respect to the AMUR code.

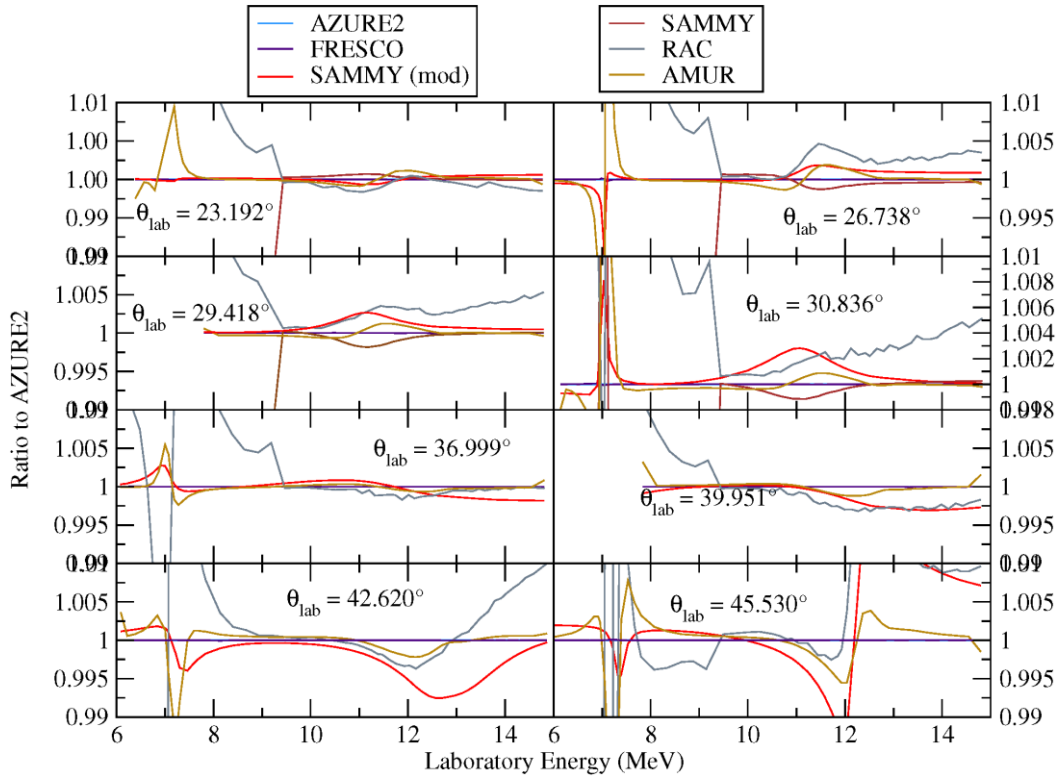


FIG. 2.4. De Boer: Comparison of calculations for the ${}^3\text{He}(\alpha, \alpha){}^3\text{He}$ reaction using the energies and angles of the Spiger and Tombrello data [2.4]. Here the vertical axis is scaled to a uniform 1%. Ratios are with respect to the AZURE2 code.

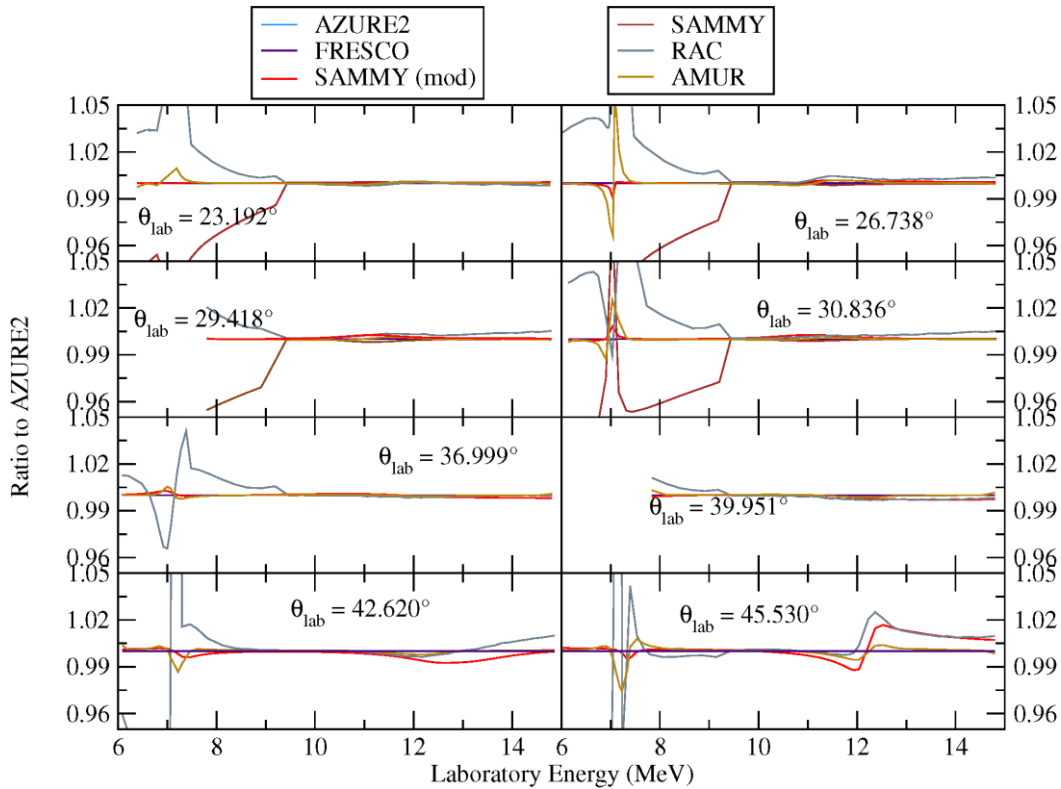


FIG. 2.5. De Boer: Comparison of calculations for the ${}^3\text{He}(\alpha, \alpha){}^3\text{He}$ reaction using the energies and angles of the Spiger and Tombrello data [2.4]. Here the vertical axis is scaled to a uniform 5%. Ratios are with respect to the AZURE2 code.

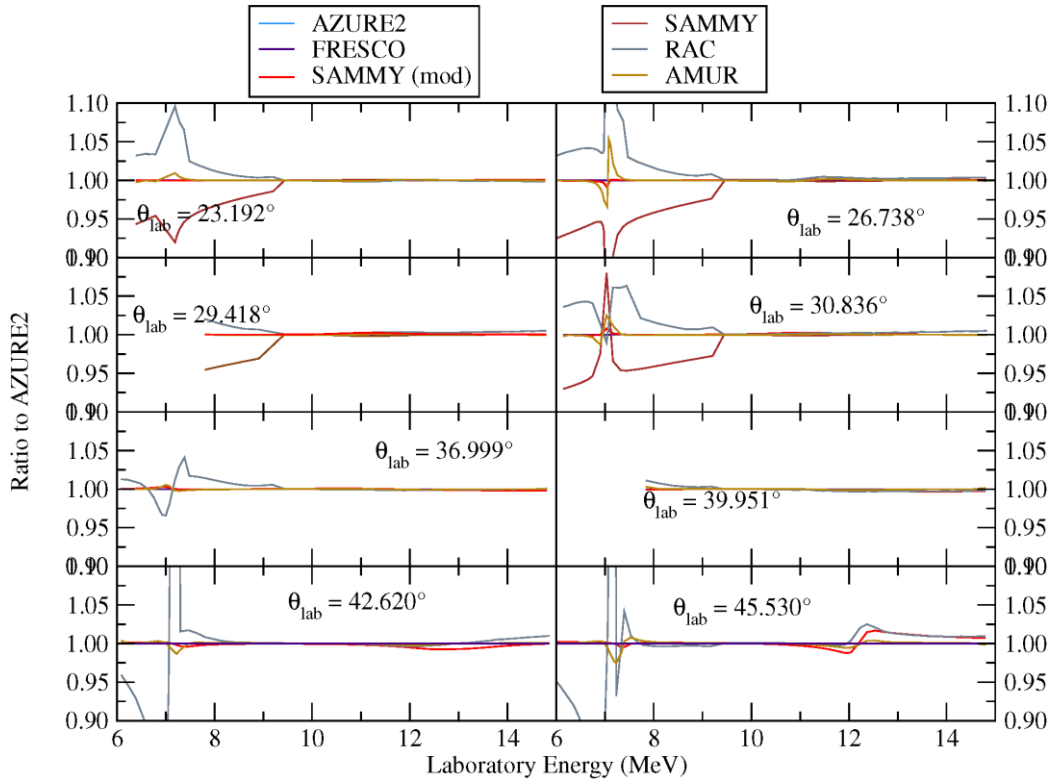


FIG. 2.6. De Boer: Comparison of calculations for the ${}^3\text{He}(\alpha, \alpha){}^3\text{He}$ reaction using the energies and angles of the Spiger and Tombrello data [2.4]. Here the vertical axis is scaled to a uniform 10%. Ratios are with respect to the AZURE2 code.

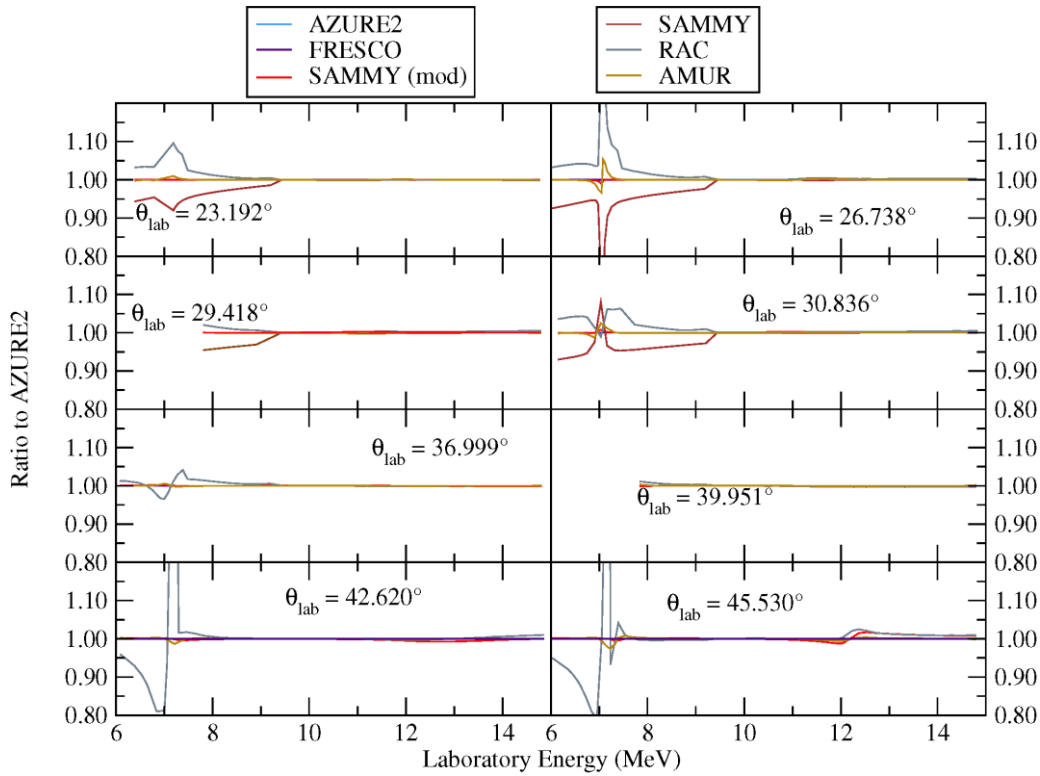


FIG. 2.7. De Boer: Comparison of calculations for the ${}^3\text{He}(\alpha, \alpha){}^3\text{He}$ reaction using the energies and angles of the Spiger and Tombrello data [2.4]. Here the vertical axis is scaled to a uniform 20%. Ratios are with respect to the AZURE2 code.

2.2. Discussion

The benchmark calculations presented in the previous section show that except for the regions around the resonances, the differences are within 0.1 - 0.3%. For the $\alpha+{}^3\text{He}$ ($\alpha+h$ from hereon) channel at higher energies the differences are higher and range from 1% to 20% (see Figs. 2.4-2.7).

The desired level of agreement is 0.1 - 0.3%, therefore more work is needed to understand the observed disagreement.

Given that these calculations can be sensitive to the Coulomb functions, one further test would be to compare the Coulomb functions calculated by each code. A simple test would be to calculate the following quantities: energy shift S , penetrability P , and hard sphere phase shifts ϕ at energies from -5 to 20 MeV for both partitions $\alpha+h$, $p+{}^6\text{Li}$.

Other checks that need to be made:

Chen's results are quite different, so he will check the formulas implemented in his code RAC. [Sec. note: After the meeting Chen communicated the results of checking his code RAC: about 10 years ago they introduced modified formulae for 'level width and energy shift' that are more suitable for multi-level multi-channel R-matrix analyses. They have published their new approach in Z.P. Chen, R. Zhang, Y.Y. Sun, T.J. Liu, Science in China (Series G) 46, 225 (2003). Furthermore, they use the integrated method to calculate the Whittaker functions. Seeing that the RAC code is using a distinctly different R-matrix algorithm compared to the other codes, Chen advised not to include RAC results in the Test 1a comparison.]

Kunieda should check the effect of interpolating at experimental energies: he should compare his Test 1a results with those obtained with his new recent code which calculates cross sections at the given energies of the experimental data without performing an interpolation.

The results of Hale for the Barnard data at low energies show slight shifts in the energies of the peaks of the resonances which could be an effect of using relativistic kinematics. Hale should provide more Test 1a calculations to complete the comparison.

Action on DeBoer: provide the values of fundamental constants and atomic masses consistent with the empirical Q-values used in Test 1a.

Completed 29.8.2018 (sent to all).

Action on Thompson: coordinate the comparison of Coulomb functions (energy shift S , penetrability P and the hard sphere phase shift ϕ).

To facilitate the comparison Thompson has prepared and sent everyone a subroutine that reads files with P , S and ϕ for the two partitions ($h+$, $p+$) and then writes them in separate files for each L as function of E .

Completed 29.8.2018.

The input file for this subroutine per quantity P , S , and ϕ should be named after each code, partition number and L value with the extension named after P , S and ϕ . Each file should contain a line for each energy with the P , S and ϕ values, respectively.

Action on all participants: Using the above subroutine to prepare requested files with S , P and ϕ and send them to Thompson for comparison.

Deadline 15.9.2018.

Action on all participants: Provide final Test 1a cross sections for all channels to DeBoer.

Deadline 15.10.2018

Thompson proposed to prepare two separate papers on: (1) verification of R-matrix calculations and (2) evaluation of ${}^7\text{Be}$. The complete title proposed for (1) is: Verification of R-matrix calculations of charged-particle reactions in the resolved resonance region for the ${}^7\text{Be}$ system (key words: Verification, benchmarking, R-matrix, charged particle reactions).

Dimitriou has prepared a preliminary outline of paper (1) which needs to be updated and then shared with the whole group so that they can include their contributions.

Action on Dimitriou: complete the first draft of the paper and share it with the group on Overleaf.

Deadline Monday, 3. 9. 2018.

Action on all participants: Prepare final draft of the paper for submission by 15.12.2018.

Action on Dimitriou: Monitor the preparation of the paper, contact EPJ A about submission, probable date, volume etc.

Deadline 30.9.2018.

3. Test 1b

The purpose of Test 1b was to compare in detail the fitting capabilities of the codes, therefore the initial conditions of Test 1a were extended to allow for background poles and were used as starting input file for fitting the ${}^7\text{Be}$ system for excitation energies up to $E_x = 8$ MeV, i.e. at energies that exclude the inelastic channels and break-up channels. The initial conditions as well as the experimental data including references and normalization conditions are given in [INDC\(NDS\)-0737](#) (Appendix).

In the following sections we present summaries of the results of Test 1b presented by the participants in this exercise.

3.1. Test 1b results

3.1.1. Test 1b results with SFRESCOX , I.J. Thompson, LLNL

Why we use R-matrix methods

In the Lane & Thomas formalism, we have the **R-matrix Theorem**. This is that, for Hermitian $H = T+V$, with $V \neq 0$ only for $r \in [0,a]$ and E -independent, then exact the scattering solutions of $HY = EY$ can be represented by a R-matrix at $r = a$ with a set of pole energies and reduced width amplitudes. In **R-matrix Practice**, we use a finite number of poles to obtain converged results. Some of the poles will be background poles outside the range of data fitting. Both the exact and practical R-matrices yield unitary S-matrix at each energy, and yield orthogonal scattering wave functions at different energies, so any proposed extension is only accepted if it has at least these properties. Both conditions come from using a Hermitian and energy-independent Hamiltonian.

Unitarity is not satisfied e.g. if imaginary damping terms, as in the Reich-Moore approximation. This is perhaps ok if a specific meaning is given to the missing flux, e.g. capture or fusion or breakup. Orthogonality is not satisfied e.g. boundary condition numbers B are not constant, as when $B = S(E)$. Both conditions are satisfied in the Brune basis, which is exactly transformable to and from standard theory (for widths not too large).

Fitting Procedure

The fitting code SFRESCOX was used to search for a χ^2 minimum for the data provided by James deBoer. The set of poles has background poles at 20 MeV in the $B = -L$ basis, with the known states at $3/2^-$, $1/2^-$ (bound in ${}^7\text{Be}$), $7/2^-$ and $5/2^-$ (twice). The bound states should be at the observed ${}^7\text{Be}$

energies, but that will not happen exactly since we are using the $B = -L$ conditions. In the end the Brune-basis bound states were constrained at the observed energy within 0.02 MeV. To improve the final fit, some broad $3/2+$ and $5/2+$ poles lower than 20 MeV were added, guided by the location of d-wave resonances in a plausible $\langle {}^3\text{He}+{}^4\text{He} | {}^7\text{Be} \rangle$ binding potential.

While searching for the best solution, the amplitudes for the background poles were found to be highly correlated in the final fit ($\chi^2 > 0.995$). Since, strictly, these are not physical observables, many of them were finally fixed, and only the norms and the middle-pole properties were varied in order to obtain the final covariance matrix. After each search run, the phase shifts were plotted on a fine energy grid to make sure no unwanted poles had crept in to the scattering region.

Comparing the experimental data, there is a clear discrepancy in the $7/2-$ resonance position in the Spiger & Tombrello alpha elastic-scattering data compared with the Barnard and the Tombrello_& Parker alpha elastic-scattering data. The Barnard data were fixed, but the energy calibration of each excitation function of Spiger+ and of Tombrello+ were fitted separately.

Final fit

A value of $\chi^2/\text{pts} = 2.884$ was obtained from the data, which increases to $\chi^2/\text{pts} = 3.037$ overall when including contributions from normalization factors differing from unity and shifts differing from zero. In the Brune basis, the $3/2-$ and $1/2-$ poles are at the constrained physical values, the $7/2-$ resonance at 2.975 MeV above threshold, and the two $5/2-$ resonances are at 5.033 and 5.593 MeV. The additional $3/2+$ and $5/2+$ resonances are at 7.79 and 6.866 MeV respectively, with most of their strength in the $p+{}^6\text{Li}$ channels. [Note: In an attempt to refit the data without the two d-wave poles, a $\chi^2/\text{pts} = 8.70$ was obtained].

The $a+h$ phase shifts are shown in F, where the resonances are very close to their Brune energies.

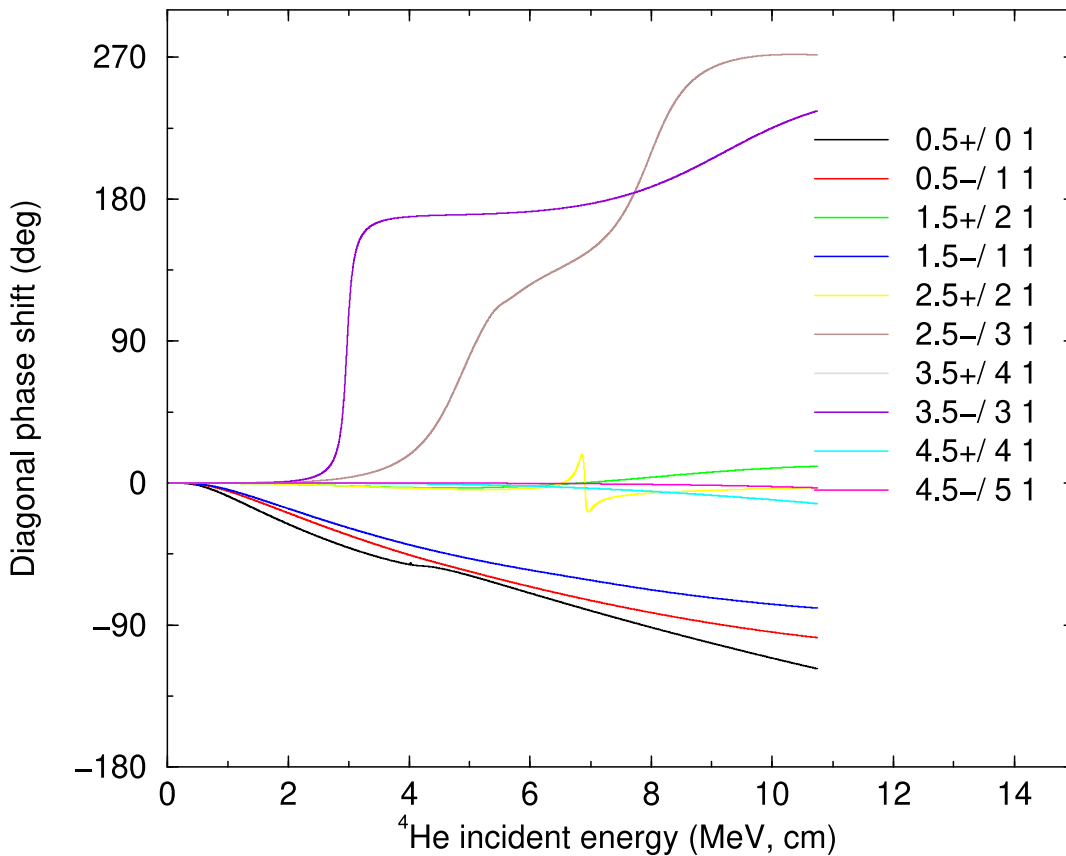


FIG. 3.1. Thompson: Diagonal phase shifts in the $a+h$ channel. The curves are for the spin groups with given J and parity.

The relative contributions to the overall fit are shown in TABLE 3.1, from each EXFOR data group.

TABLE 3.1. Contributions to the fit quality from each experimental data set.

Dataset	Chisq/pts	av norm	av shift (MeV)
Barnard_aa.dat	0.967	0.990	
Elwyn_pa.dat	4.317	1.133	
Fasoli_pp.dat	3.895	0.996	
Harrison_pp0.dat	5.489	1.156	
Lin_pa.dat	3.885	1.305	
McCray_pp.dat	3.842	1.122	
Mohr_aa.dat	3.481	0.956	
Spiger-A1094004-lab_aa.dat	2.633	0.929	-0.048
Spiger-cm_ap0.dat	1.419	1.004	
Tombrello_aa.dat	3.559	1.080	-0.036

A series of figures showing the evaluation curves with each data set and its statistical error bars is presented in the following. The captions show the file name which includes the specific energy or angle curve. After the name is the normalization shift and (for Spiger and Tombrello the energy shift). After the @ sign is given the χ^2 /pts for each curve.

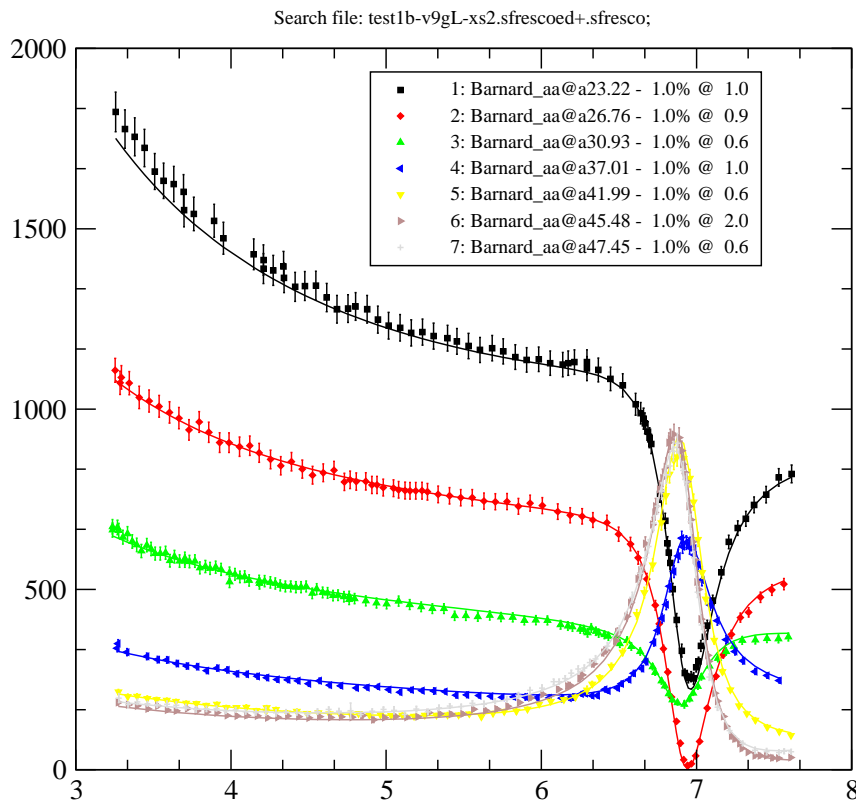


FIG. 3.1. Thompson: **Barnard_aa data**

Search file: test1b-v9gL-xs2.sfrescoed+.sfresco;

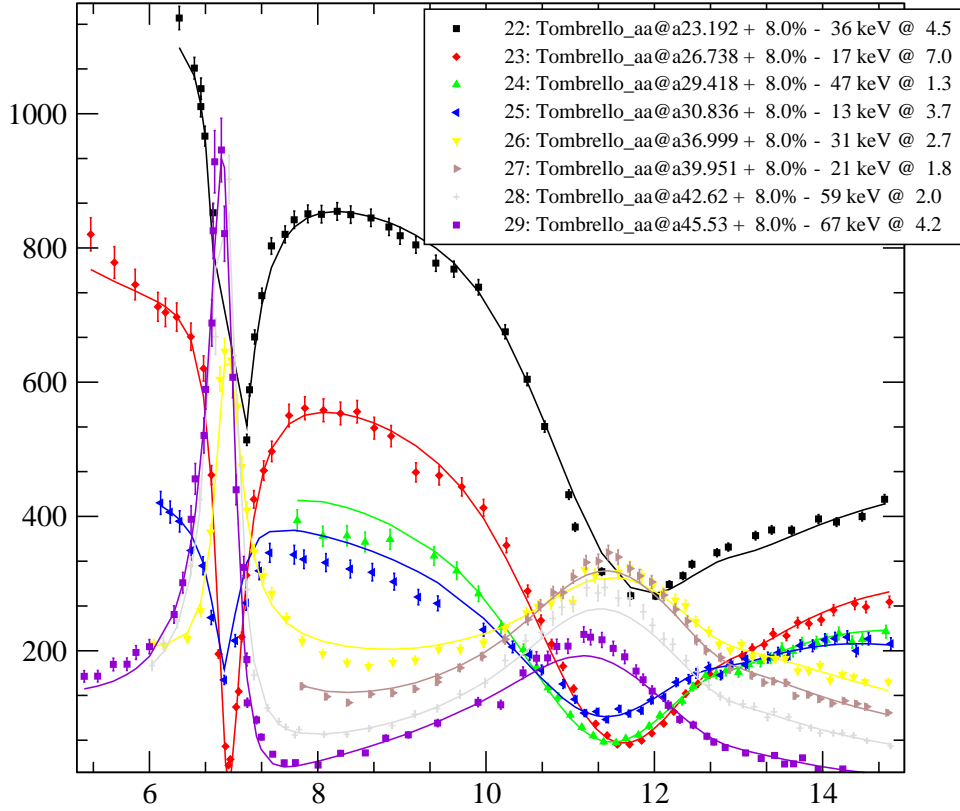


FIG. 3.2. Thompson: **Tombrello_aa data**

Search file: test1b-v9gL-xs2.sfrescoed+.sfresco;

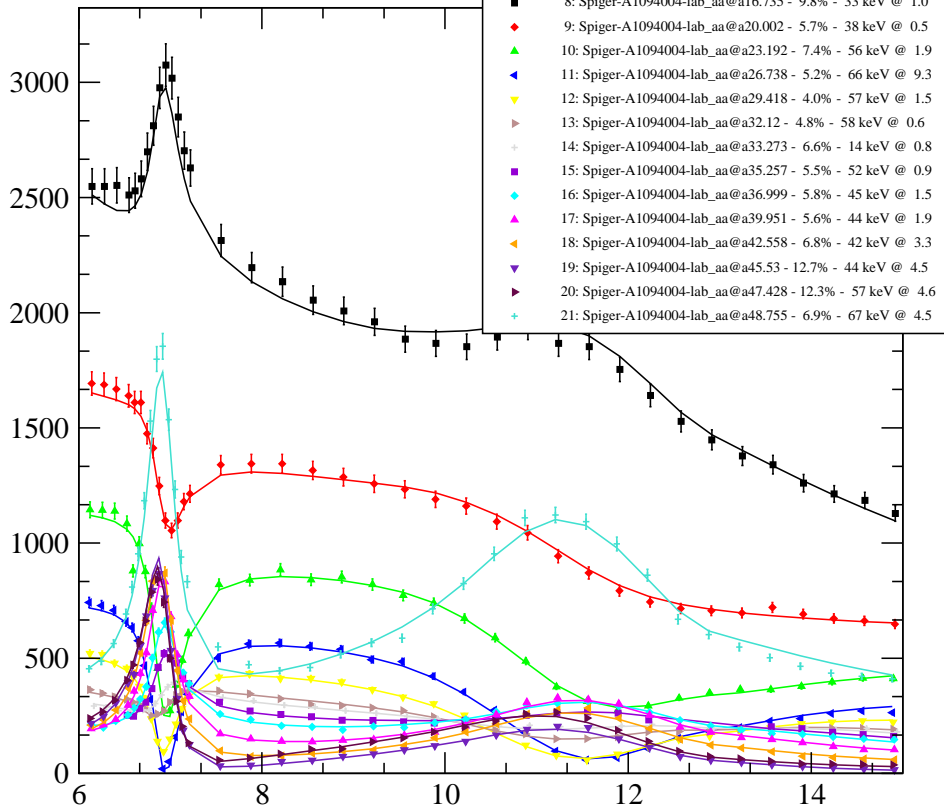


FIG. 3.4. **Spiger_aa data**

Search file: test1b-v9gL-xs2.sfrescoed+.sfresco;

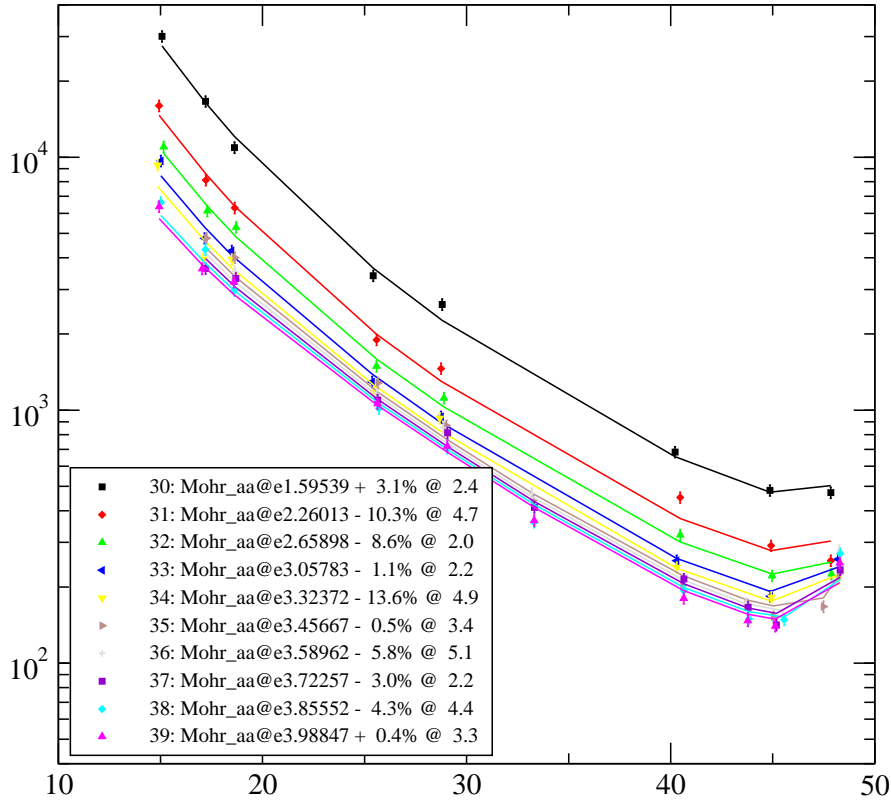


FIG. 3.3. Thompson: *Mohr_aa* data

Search file: test1b-v9gL-xs2.sfrescoed+.sfresco;

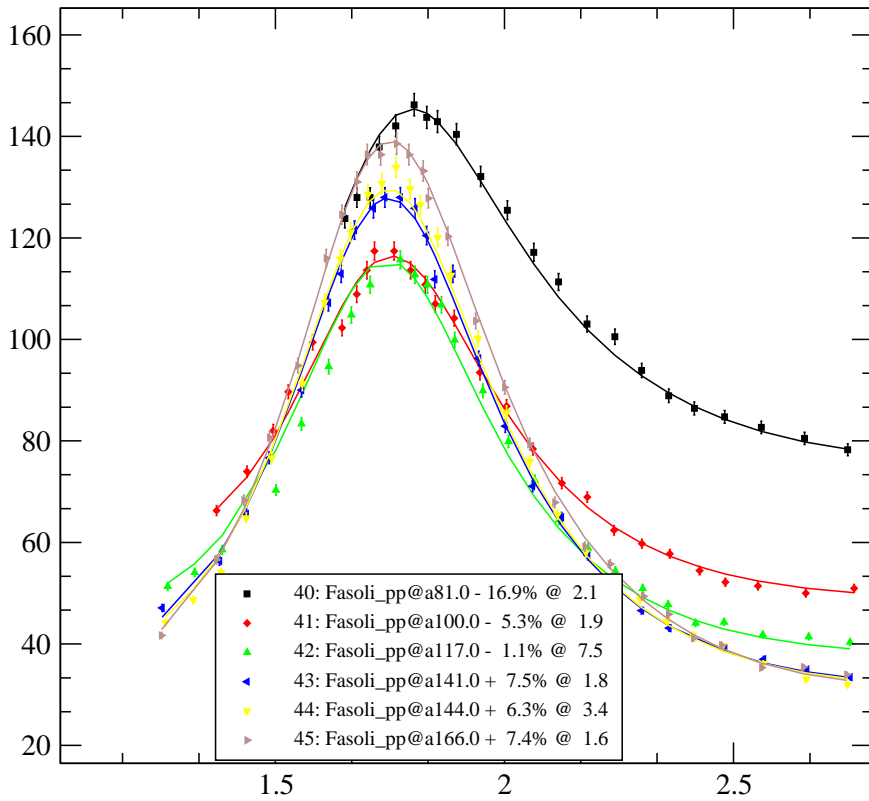


FIG. 3.4. Thompson: *Fasoli_pp* data

Search file: test1b-v9gL-xs2.sfrescoed+.sfresco;

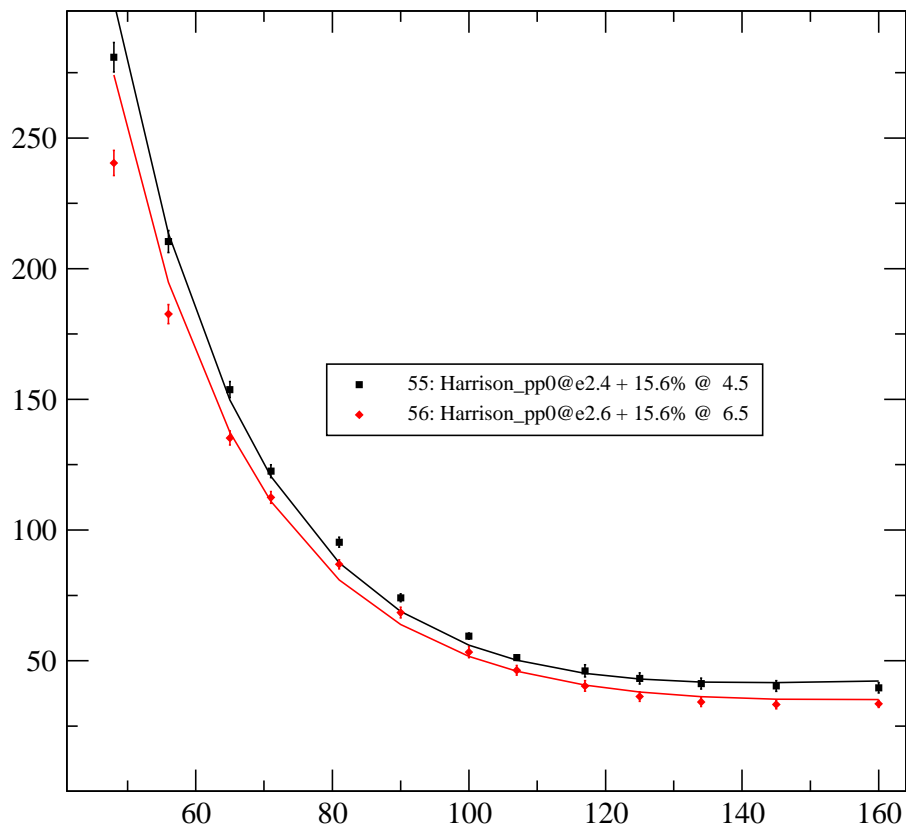


FIG. 3.5. Thompson: **Harrison_pp0.data**

Search file: test1b-v9gL-xs2.sfrescoed+.sfresco;

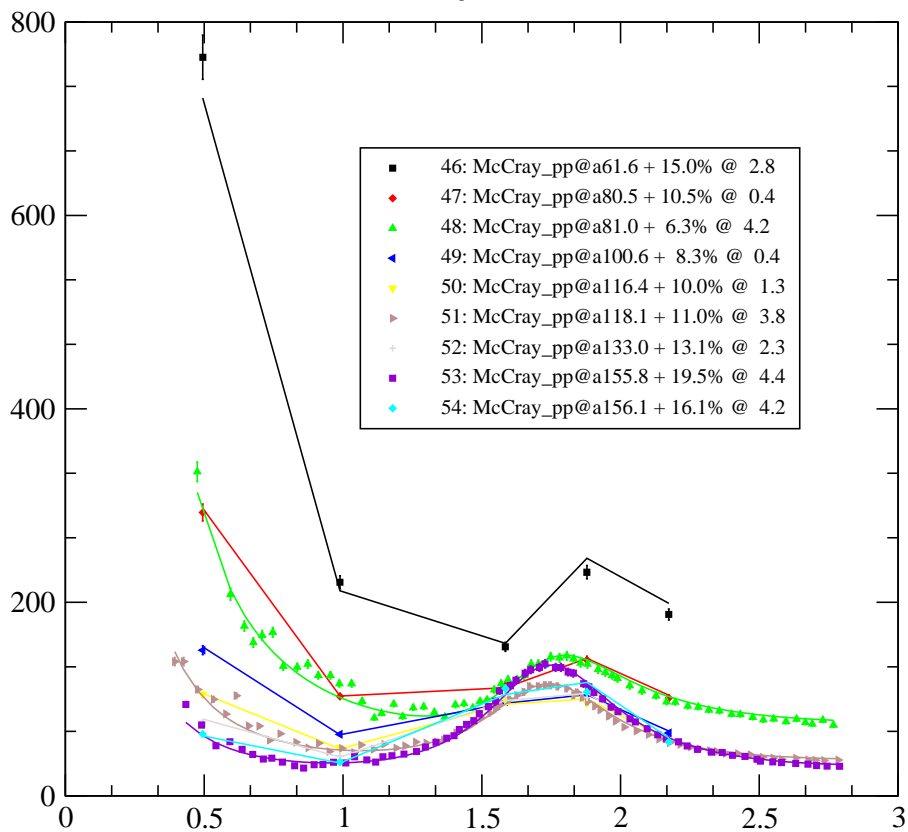


FIG. 3.6. Thompson: **McCray_pp.data**

Search file: test1b-v9gL-xs2.sfrescoed+.sfresco;

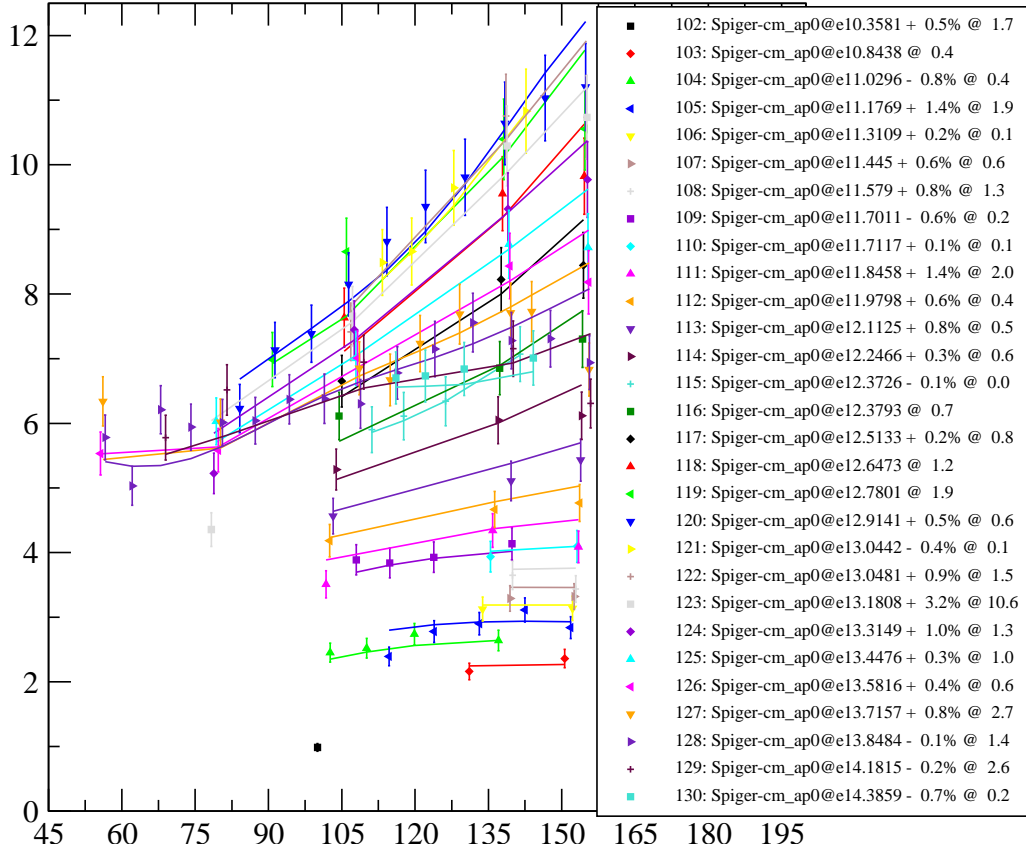


FIG. 3.9. Thompson: *Spiger-cm_ap* data

Search file: test1b-v9gL-xs2.sfrescoed+.sfresco;

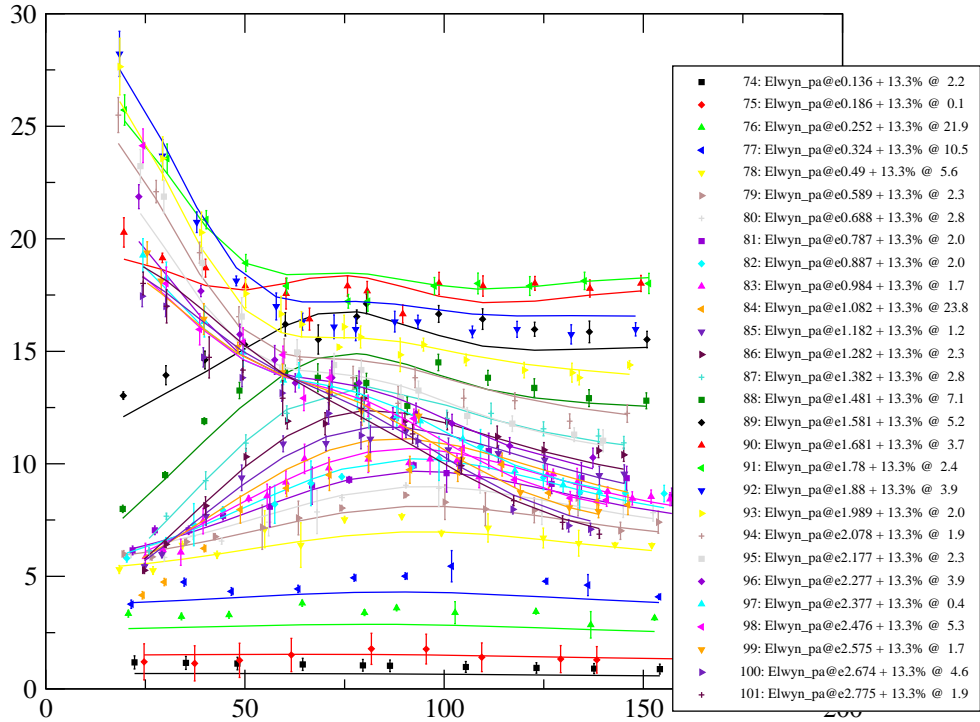


FIG. 3.7. Thompson: *Elwyn_pa* data

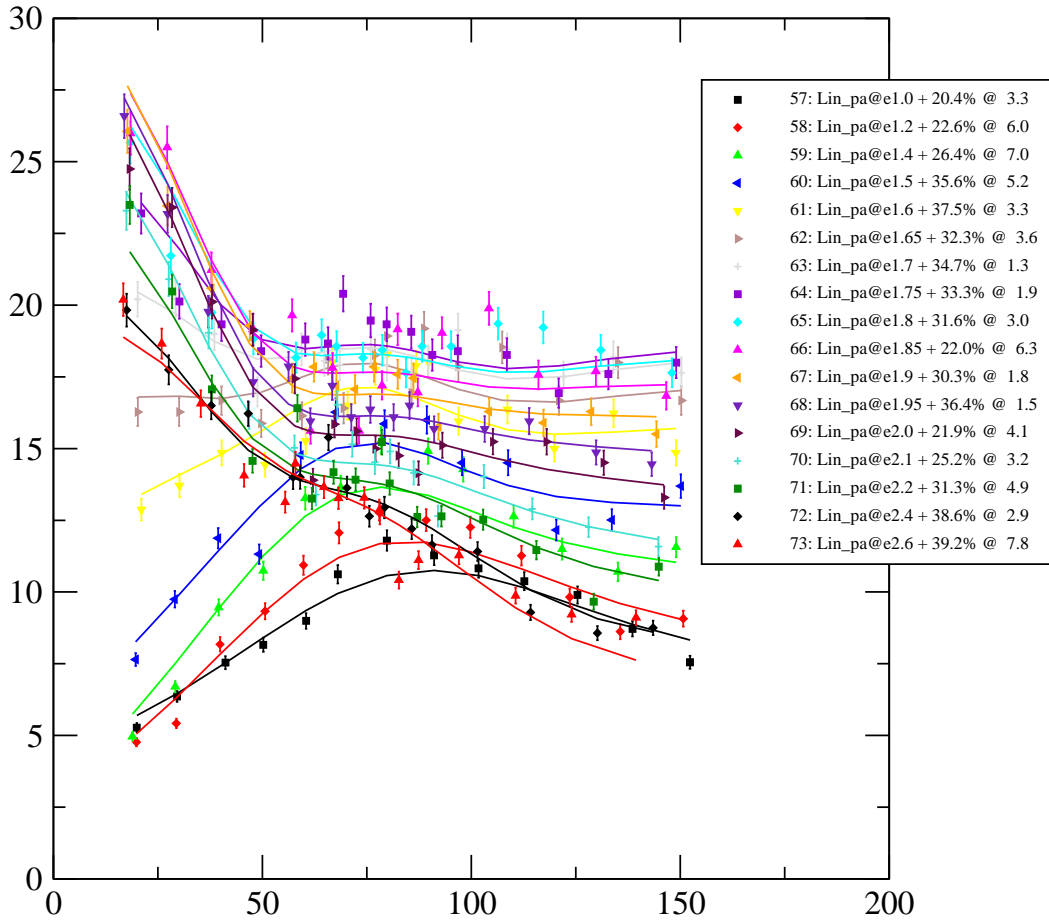


FIG. 3.8. Thompson: *Lin_pa* data

At the end, the SFRESCOX parameter output file was converted into an GNDS evaluation file using Ferdinand.py, and was then used by the validation code validateWithX4plots.py to compare that evaluation with data directly from EXFOR. Although data renormalizations and energy shifts were not included, good comparisons were obtained except for the Lin data (which is wrongly labeled in EXFOR) and for 3 energies in the Elwyn data (2.277, 2.377, 2.476 MeV) which are wrongly plotted in the original paper.

Discussion: The problem is that there is a great difference between Lin and Elwyn pa data. Comparison with Chen's analysis shows that it is important to handle the data in the same way.

3.1.2. Test 1b results with AZURE, R.J. deBoer, Univ. Notre Dame

Following the strict constraints set forth for Test 1b, a good fit could not be obtained. The fit was started by taking Kunieda's fit values from Test 1a and also adding the additional known bound state level at $E_x = 0.42908$ MeV in ${}^7\text{Be}$. The fit was done in the Brune basis, so that some parameters could be more easily fixed at known experimental values, but then these parameters were transformed into the $B = -L$ basis as this was the one that the parameters were to be reported in.

Fitting with AZURE2 was performed using MINUIT2. Covariance and correlation matrices are calculated with the MINOS routine of MINUIT2.

It was quickly apparent that fitting with just the observed levels in the literature would not produce a good fit to the data. In accordance with the constraints of Test 1b, background states were then added at $E_x = 20$ MeV (although the intent that these energies should be excitation energies was erroneously left out of the instructions). A background state was added for each $J\pi$ up to $9/2^-$, which

was needed to produce all of the alpha+h L channels up to $L = 4$. This also produced up to $L = 1$ channels for p+6Li as required by the exercise. The background state contributions were not put in all at once, but were included one by one starting with the lowest $J\pi$. In addition, only those channels with the lowest L were initially included. Starting with $1/2^-$, only a small improvement was obtained, but adding in the $1/2^+$ contribution improved the fit substantially. Likewise, adding the $3/2^-$ level had little effect, while adding the $3/2^+$ again had a large effect. The remainder of the levels up to $9/2^-$ were then also added one by one. While each improved the fit somewhat, they didn't have nearly the effect that adding the $1/2^+$ and $3/2^+$ background levels had.

Even with the improvement of the background levels, the fit still had a very large χ^2 . Higher L channels were then also considered for each $J\pi$. This did result in some improvement, more with the negative parity states, but still did not give a very good χ^2 . During this process it was observed that many of the widths of the background states would run off to very large values and that they were highly correlated with each other and with the higher order l partial widths of the real levels. The two $5/2^-$ levels were found to be particularly troublesome. The $L = 3$ proton channels were found to be highly correlated with the widths of the background levels.

In addition to the background states, the asymptotic normalization coefficients ANC (which can be directly related to their reduced widths) of the subthreshold states were also allowed to vary. These were likewise found to be highly correlated with the parameters of the background states both in the alpha and proton channels. Finally, the alpha ANCs were fixed to values determined from capture experiments ($ANC_{GS} \alpha = 3.7 \text{ fm}^{-1/2}$ and $ANC_{FES} \alpha = 3.6 \text{ fm}^{-1/2}$). Proton ANCs can also be determined from ${}^7\text{Li}(p, \gamma)$ data but these were not considered.

Correlations between parameters were observed both by noting different values by doing various different fits and quantitatively by calculating the correlation matrix with MINOS. These calculations initially caused MINOS to crash. The tactic used was to fix all but one of the parameters at their best fit values and run MINOS, then allow an additional parameter to vary and repeat. When a newly freed parameter would cause MINOS to crash, that parameter would be eliminated from the fit and a refit performed. If the resulting χ^2 was similar to the best fit value, the parameter was eliminated, if the χ^2 was found to be worse, the parameter was kept but its value was fixed. Following these procedures each of the fit parameters were tested and the covariance matrix was eventually calculated. In addition to the level fit parameters, the normalization factors were also fixed during this procedure. However, when a set of fit parameters was obtained that resulted in a successful calculation of the covariance matrix, these parameters were then also included in the calculation. This calculation was successful. Now looking at the correlation matrix, parameters with large correlations were also examined (>0.9). Further parameters were then fixed or eliminated so that no correlation was >0.9 .

While many different fitting schemes were attempted, within the constraints imposed by the exercise, a good fit could never be obtained. Some examples of the fitting are given in the Figs. (3.12-3.15). The main conclusions of this work are that the background state widths are highly correlated, making it practically difficult to achieve a good fit. In addition, the constraints imposed by the exercise were too stringent. Fits that violate the constraint of a single background state at $E_x = 20$ MeV (that is a second background state at a different energy) seem to be necessary to achieve a good fit. Additionally, previous fits that used higher energy data and included the p_1 channel also showed promising results.

Discussion: Remark - the ${}^3\text{He}$ -data are very bad. Larger channel radius may help to get transformable parameters. Spiger and Parker data uncertainties are likely underestimated.

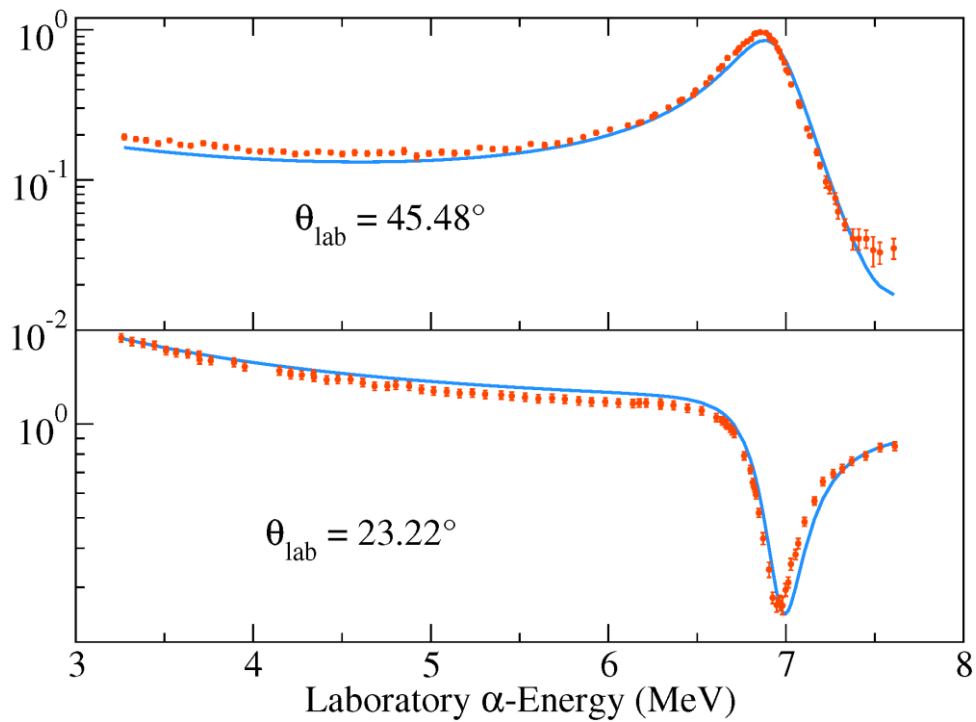


FIG. 3.12. DeBoer: Barnard (α,α) data.

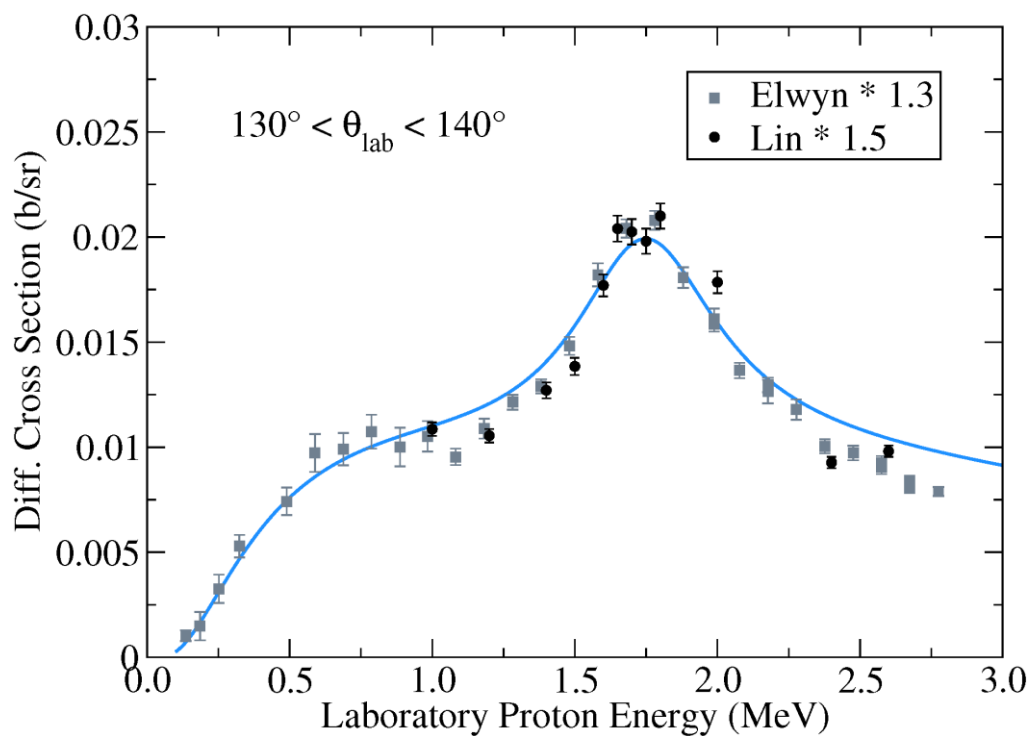


FIG. 3.13. DeBoer: Elwyn (p,α) and Lin (p,α) data.

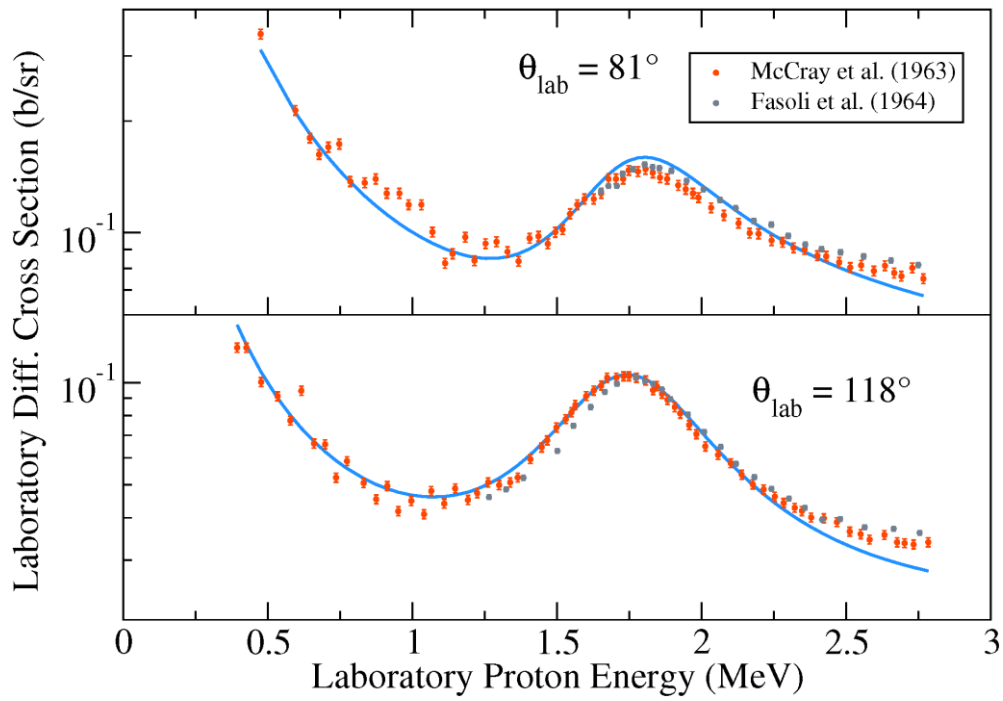


FIG. 3.14. DeBoer: McCray (p,p) data.

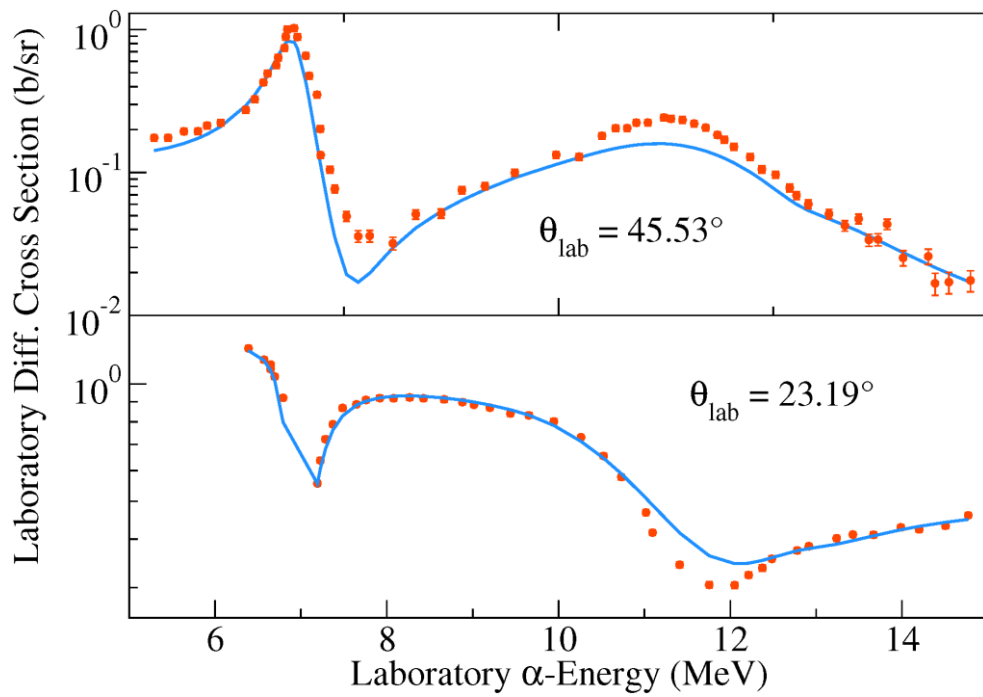


FIG. 3.15. DeBoer: Tombrello (α,α) data.

3.1.3. Test 1b results with AMUR, S. Kunieda, JAEA

Updates of the AMUR code: Since the last meeting, several updates were made in the AMUR code [1] to ensure consistency with the other codes as much as possible. The updates are listed as follows.

- (1) The reaction Q-values are calculated by the mass difference in the original code. Optionally, those values are also calculated by the separation energies provided as the external information.
- (2) The coulomb wave and the Whittaker functions had been calculated by using GSL (GNU Scientific Library). The code is now able to use a subroutine that is taken from an optical model code POD [2] for the Coulomb function. The Whittaker function can also be calculated by his own subroutines that is based on the integral method.
- (3) In the fitting procedure, cross-sections were not calculated at exactly the same points of experimental data, instead the interpolation was used in the original version. This situation was improved by adding experimental energy/angle points to the initial nodes for the reconstruction.

The differences in the calculations performed with the original code and the other codes used to be in the order of several percent at maximum. The difference has now become less than ~1% once the update described in item (1) was made. It was found that there is no impact from the update of the Coulomb and Whittaker function routines (2) at least for the present test case (Test 1a/Test 1b). In the near future, the impact of the update described in item (3) needs to be checked.

Fitting procedure: The Kalman filtering method (same as in the KALMAN/SOK code) [3], which is equivalent with the generalized least-square method, was used for the parameter search. All the cases described in the following were performed in the logarithmic space to reduce number of the iterations. In the fitting, only the diagonal elements of experimental covariance were considered. The covariance matrix of the resonance parameters was also obtained during the fitting procedure.

R-matrix analysis for Test 1b: Three cases, which are called Case-1, 2 and 3, were calculated to investigate differences among the parameterizations in the R-matrix analysis for Test 1b.

Case-1: The condition of Test 1b is followed exactly, except for the parameters excluded due to very low sensitivity to the cross-sections.

Case-2: R-matrix fit is started from parameter set provided by I. Tompson in which additional poles ($3/2+$, $5/2+$) are assumed. In order to have the same condition of I.T., all the parameters of the distant poles were fixed in the fitting procedure.

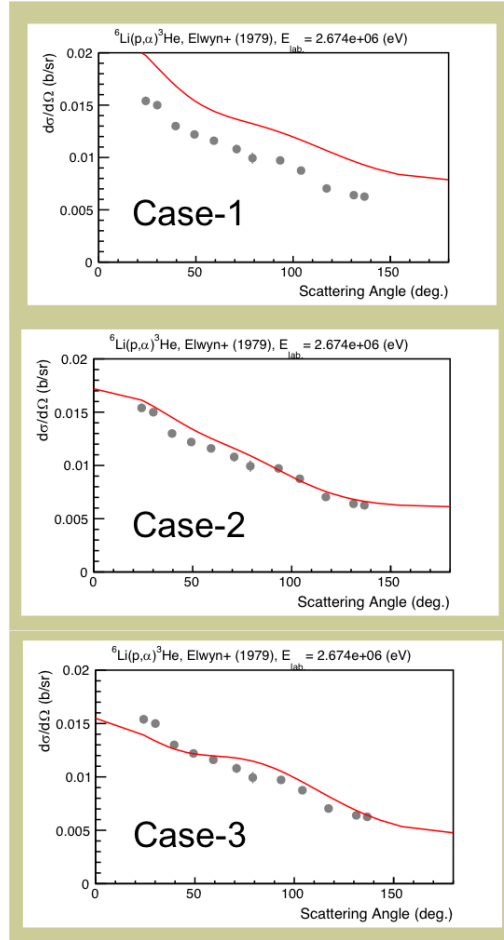


FIG. 3.16. Kunieda: Comparison of fitting results among the different cases on the ${}^6\text{Li}(p,\alpha)$ differential cross-sections at 2.674 MeV.

Case-3: In Test 1b, the independent distant poles are assumed for (p,p) and (α,α) channels for each J^π group. Such new additional poles are preliminary set at 20 MeV in the present analysis. It should be noted that there is not any correlation between the new poles of (p,p) and (α,α).

It was found that the χ^2/N values obtained are 19.5, 5.6 and 7.2 for Case-1, 2 and -3, respectively. One example of the comparison of cross-section is illustrated in Fig. 3.15, where the results of the three cases for ${}^6\text{Li}(p,\alpha){}^3\text{He}$ are compared with the experimental data of Elwyn et al. Firstly, it was found that only the Test 1b condition is not enough to achieve a reasonable fit to experimental data. This fact suggests that additional poles are certainly necessary as it was assumed in Case-2 and -3. Example of the normalization values obtained are also listed in Table 3.2 where the Case-2 and -3 show very similar values while Case-1 is rather different from the others. Figure 3.16 illustrates correlation matrices for ${}^6\text{Li}(p,\alpha)$ differential cross-sections at c.m. angles 5, 30, 90, 120, 150 and 180 degrees. It is found that the cross sections are fully correlated at middle angles while they become rather local at small and large angles.

TABLE 3.2. Example comparison of normalization among the cases

	Case-1	Case-2	Case-3
Barnard1964	$0.99809 \pm 0.180 \%$	$1.00316 \pm 0.144 \%$	$1.00765 \pm 0.185 \%$
Tombrello1963	$0.92484 \pm 0.198 \%$	$0.92956 \pm 0.172 \%$	$0.94827 \pm 0.197 \%$
Harrison1967	$0.74992 \pm 0.498 \%$	$0.86825 \pm 0.492 \%$	$0.86693 \pm 0.475 \%$
Elwyn1979	$0.79055 \pm 0.549 \%$	$0.88509 \pm 0.233 \%$	$0.86271 \pm 0.623 \%$

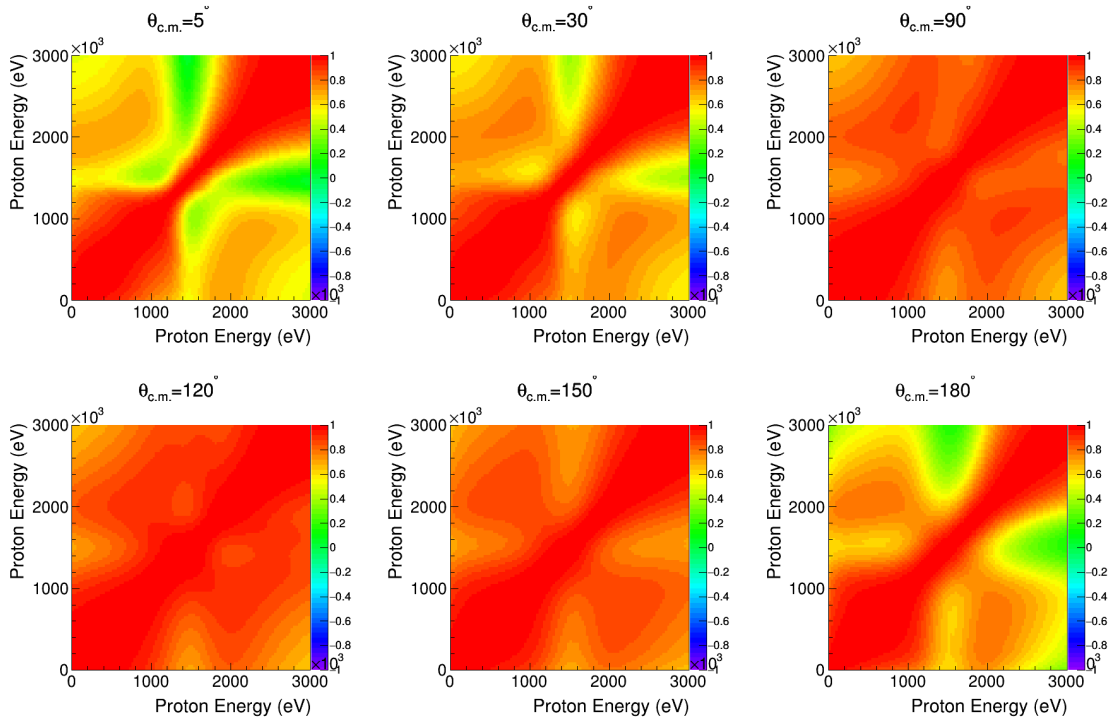


FIG. 3.17. Kunieda: Correlation matrices for ${}^6\text{Li}(p,\alpha)$ differential cross-sections at different angles.

References

- [1] S. Kunieda et al., Nuclear Data Sheets **123**, 159 (2015).
- [2] A. Ichihara et al., JAERI-Data/Code 2005-004 (2005).
- [3] T. Kawano et al., J. Nucl. Sci. Technol. (Tokyo) **37**, 327 (2000).

Discussion: the correlation matrices shown are blocks on the diagonal and do not show any cross-channel correlations. Can these be produced as well? What about producing covariance matrices? Hale mentioned that he stores them in pointwise format not resonance parameters.

3.1.4. Test 1b results with RAC, Z. Chen, Tsinghua University of Beijing

Eight fitting schemes have been done for the given data-base of Test1b, in which, the scheme with the original level structure given in **test1b** did not work, the $\chi^2/\text{freedom}$ is 26.2; the scheme with the improved level structure used in **test1a** did not work either, the $\chi^2/\text{freedom}$ is 16.2; then 6 improved different schemes of level structure were used to get the best fitting; it was found that the scheme of **Chen3-10JP-19L** has $\chi^2/\text{freedom}$ 1.042, the scheme of **Chen6-10JP-28L** has $\chi^2/\text{freedom}$ 0.884.

This shows that the level structure used plays a dominant role.

The ${}^6\text{Li}(p,p){}^6\text{Li}$ dataset of McCray 1961 [2.3] at 90 deg. is added to the experimental database, because they are the most accurate experimental data available for the ${}^7\text{Be}$ system. The systematic error given in the paper of McCray is taken as a constraint for the normalization, i.e. the modification of the scale of the experimental data does not exceed the systematic error given in the paper in most of the cases fitted herein. The whole fit looks good, the mean chi-square is about 0.884, and for most of the data the calculated values are close to the experimental values. The serious problem which existed in the initial input file (Chen-start-10JP-28L) has been removed. When that original file was used, the first peak of ${}^6\text{Li}(p,p){}^6\text{Li}$ with $J\pi = -5/2$ was overestimated and one also observed 2 peaks in some excitation functions. The reason was that 2 resonances existed with $J\pi = -5/2$, which produced strong interference. In theory, if 2 poles exist with the same $J\pi$ and there are only one or two open reaction channels, the interference among these two poles will be rather strong if they are very close in energy. In Test 1b there are only 2 reaction channels ${}^6\text{Li}(p,p){}^6\text{Li}$ and ${}^6\text{Li}(p,{}^3\text{He}){}^3\text{He}$ since the open

reaction channel ${}^6\text{Li}(p, g){}^7\text{Be}$ is ignored, so the two poles show strong interference. It was found that this strong interference always occurs even if different test level-structures are used. In this work, we have implemented the reduced R-matrix theory and used the parameter 'width of reduced channel' to represent the ${}^6\text{Li}(p, g){}^7\text{Be}$ and other open channels which were previously ignored. We find that when we do that, the strong interference effects disappear.

In the following figures, 'Ori' means the original experimental data, 'Nor' means normalized data. N and S mean normalization factor and shape factor, respectively.

In this fit the ${}^3\text{He}({}^4\text{He}, {}^4\text{He}){}^3\text{He}$ and ${}^6\text{Li}(p, p){}^6\text{Li}$ are the dominant channels whereas the fitting values of ${}^3\text{He}({}^4\text{He}, p){}^6\text{Li}$ and ${}^6\text{Li}(p, {}^4\text{He}){}^3\text{He}$ depend on ${}^3\text{He}({}^4\text{He}, {}^4\text{He}){}^3\text{He}$ and ${}^6\text{Li}(p, p){}^6\text{Li}$.

3.1.4.1. ${}^3\text{He}({}^4\text{He}, {}^4\text{He}){}^3\text{He}$

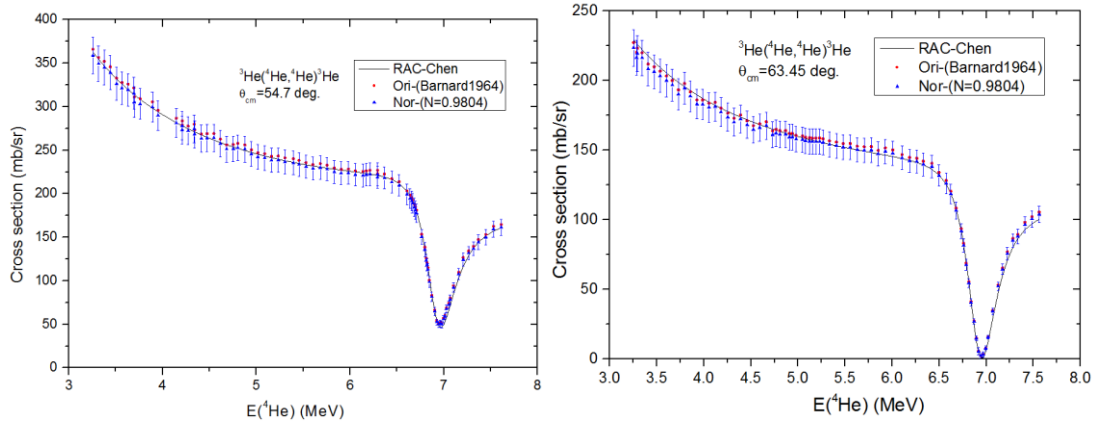


FIG. 3.18. Chen

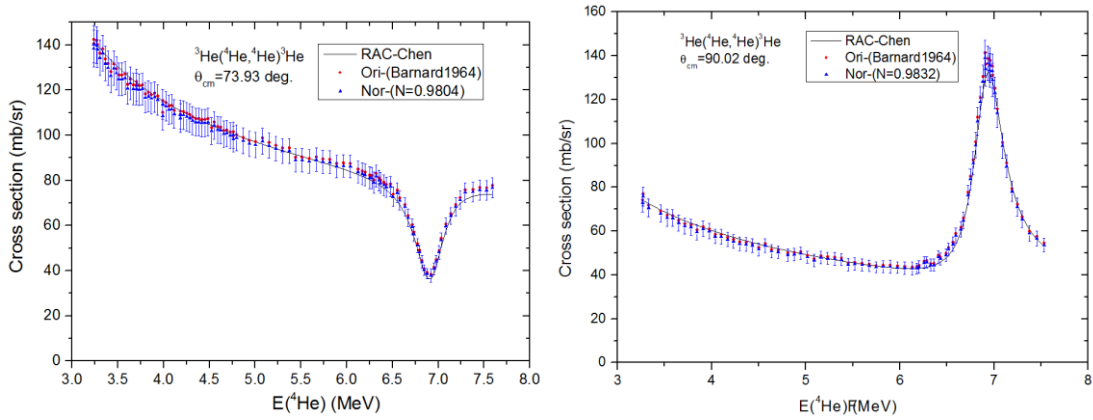


FIG. 3.19. Chen

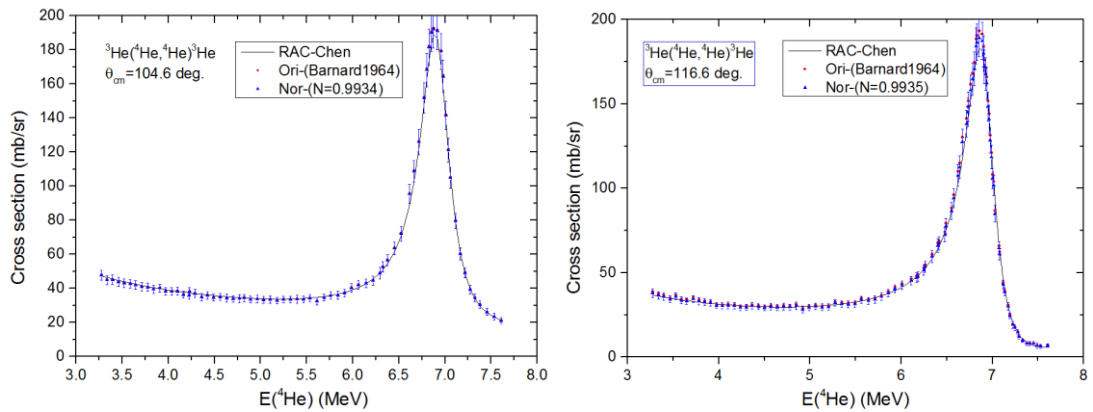


FIG. 3.20. Chen

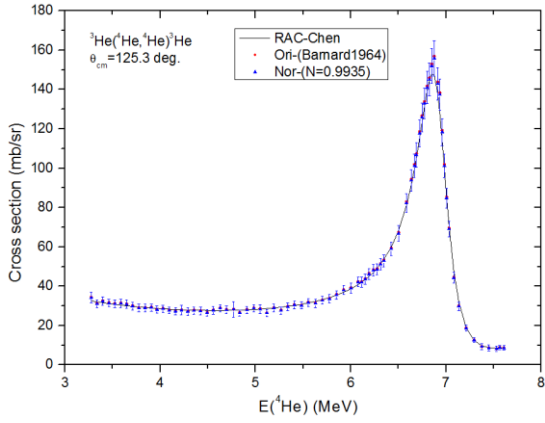


FIG. 3.21. Chen

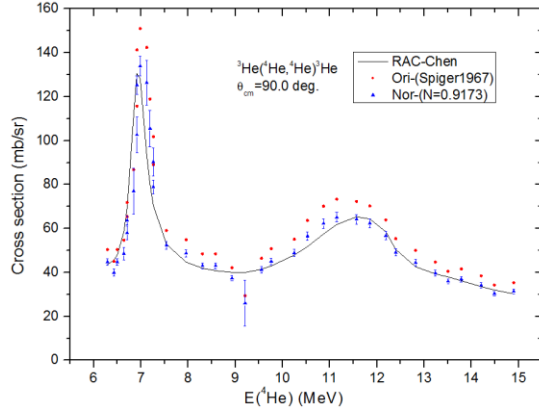
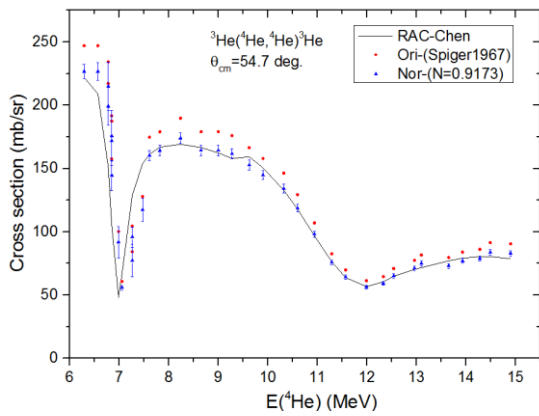


FIG. 3.22. Chen

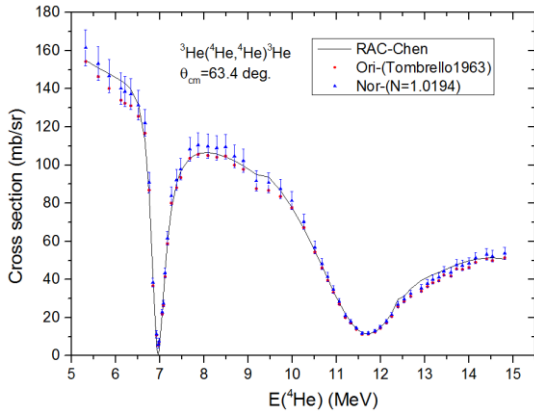
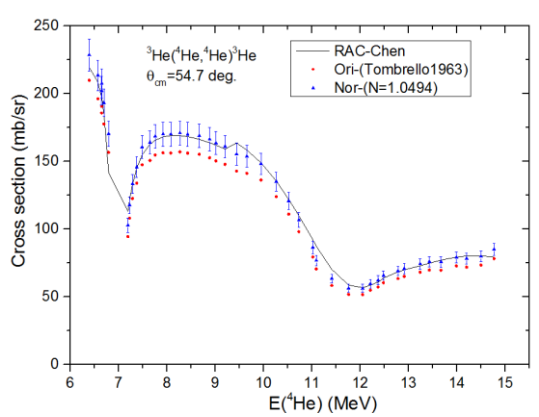


FIG. 3.23. Chen

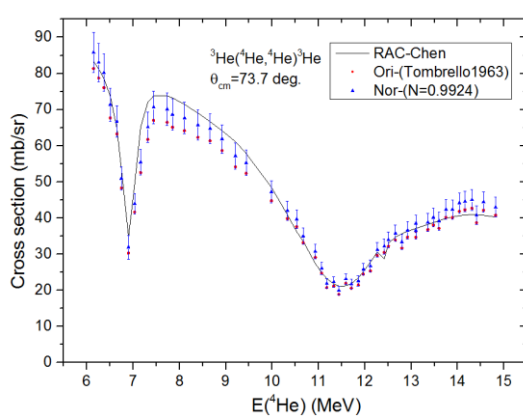
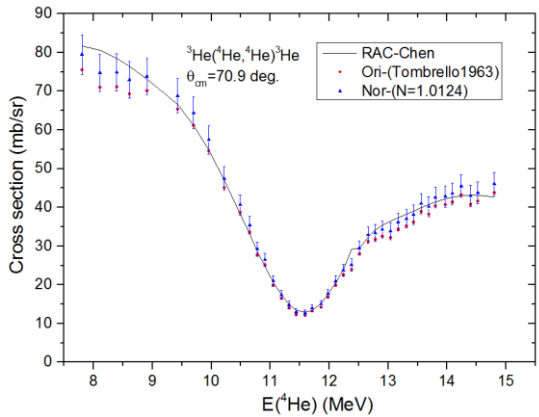


FIG. 3.24. Chen

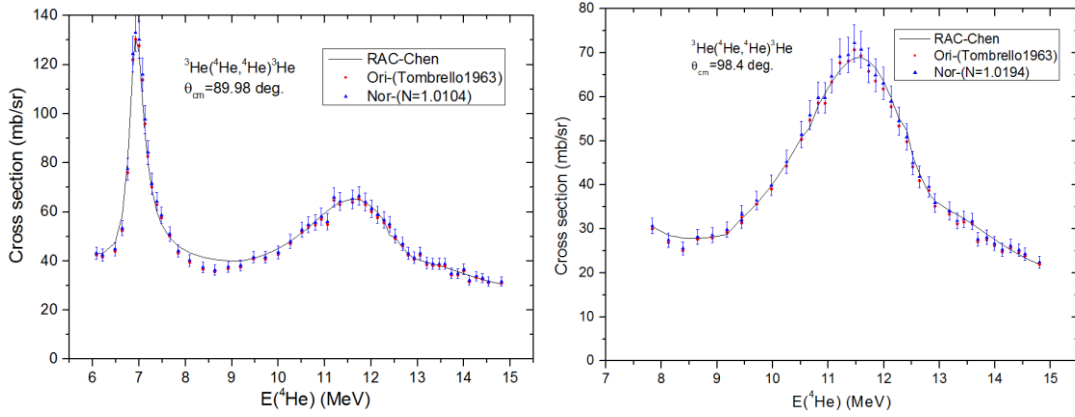


FIG. 3.25. Chen

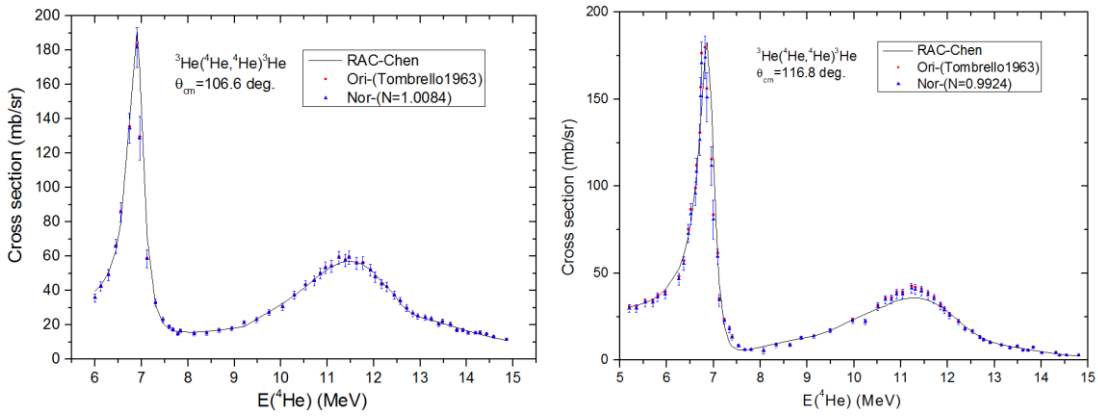


FIG. 3.26. Chen

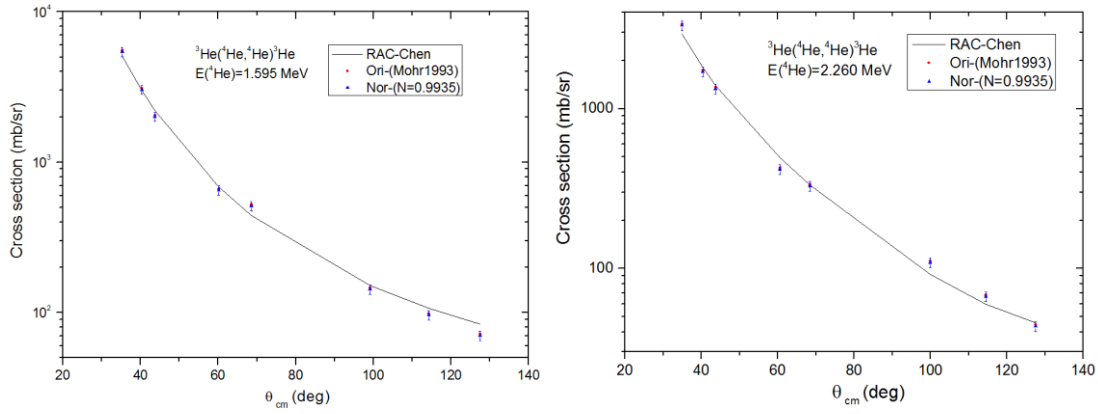


FIG. 3.27. Chen

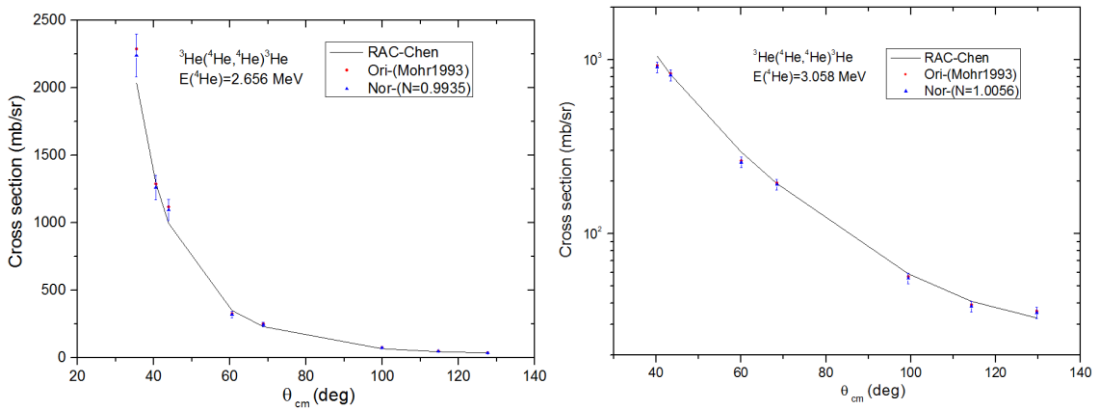


FIG. 3.28. Chen

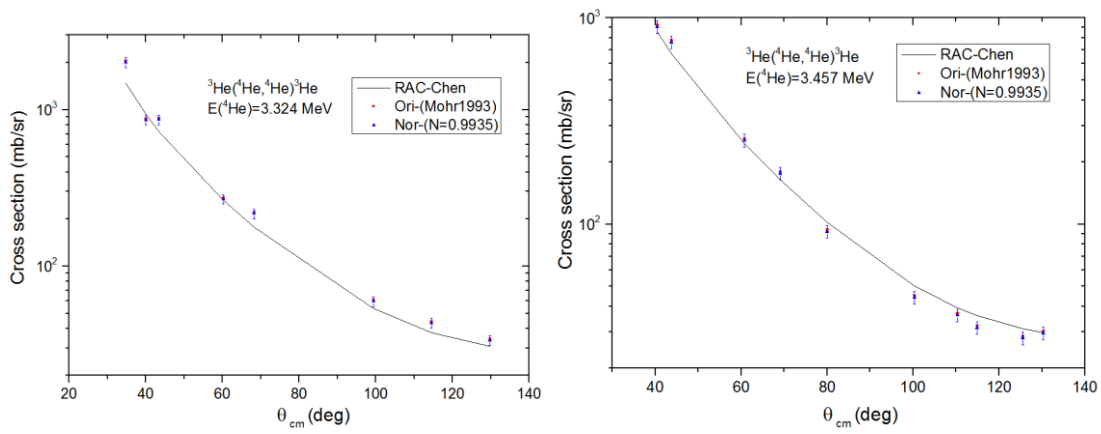


FIG. 3.29. Chen

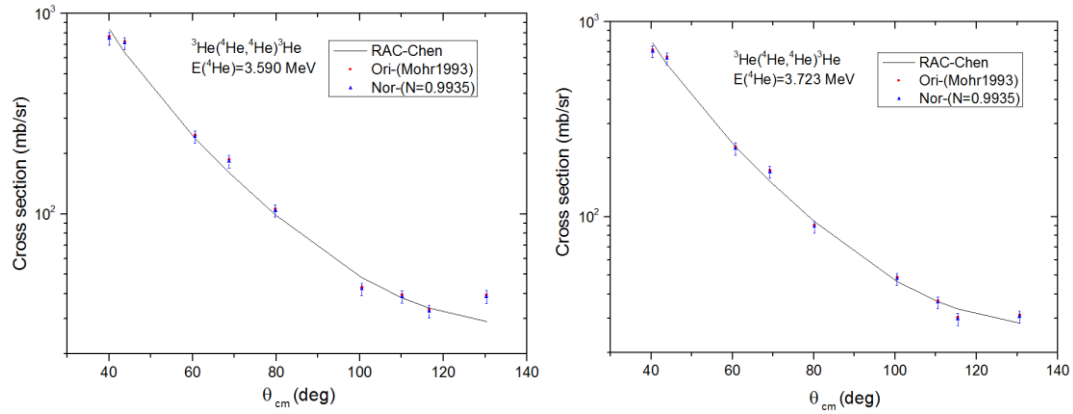


FIG. 3.30. Chen

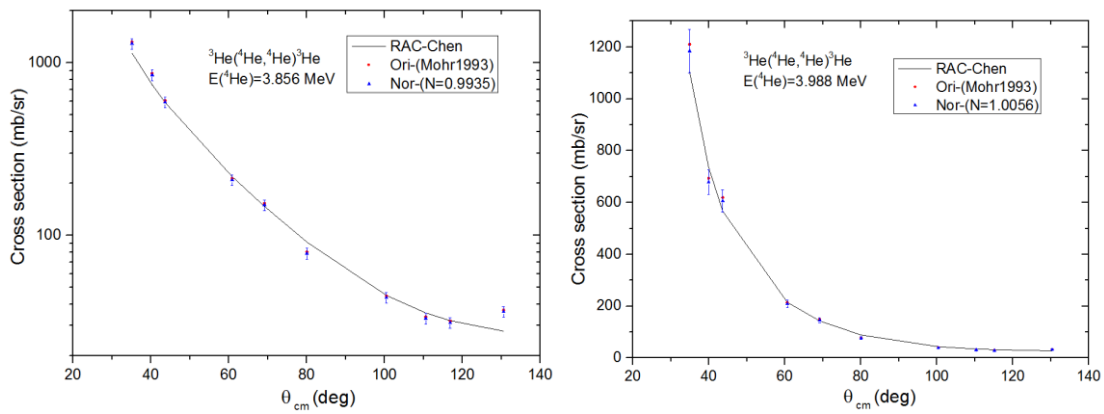


FIG. 3.31. Chen

3.1.4.2. ${}^6\text{Li}(p, p){}^6\text{Li}$

All fits look very good.

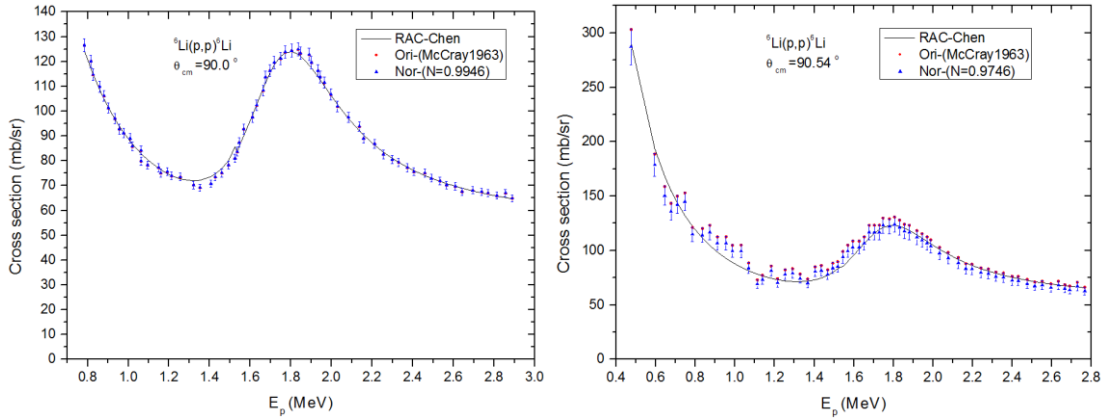


FIG. 3.32 Chen The ${}^6\text{Li}(p, p){}^6\text{Li}$ dataset at 90 deg of McCray1961 (Left) is added to Test 1b, because it is the most accurate absolute experimental data with statistic error near 0.5% in the ${}^7\text{Be}$ system.

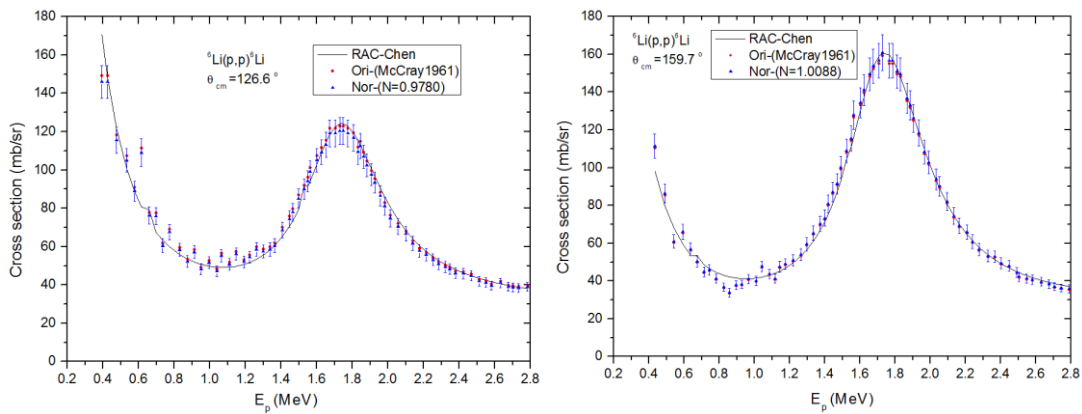


FIG. 3.33. Chen

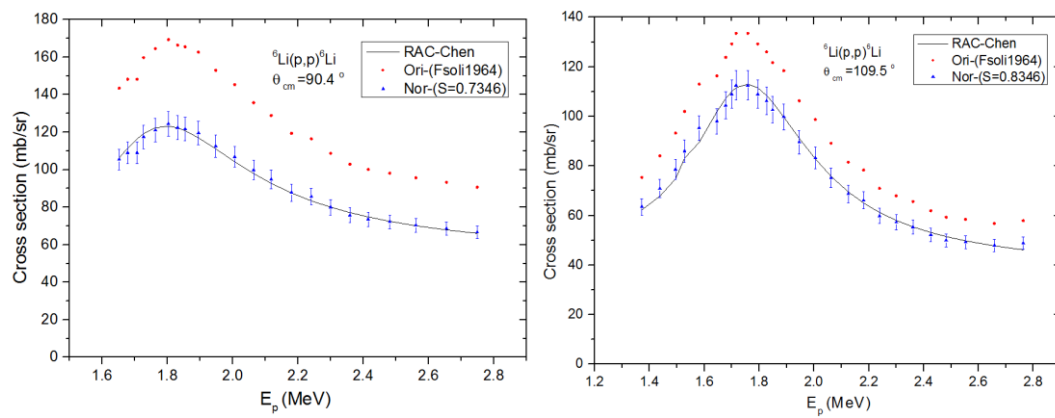


FIG. 3.34. Chen

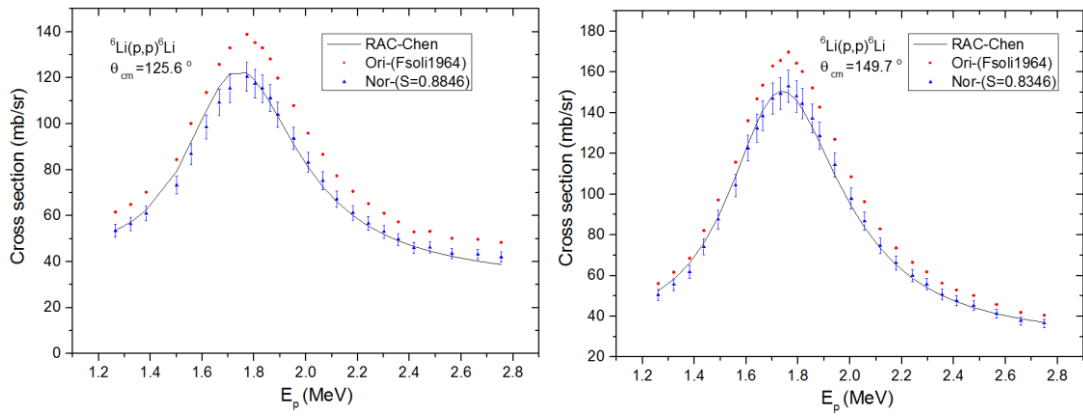


FIG. 3.35. Chen

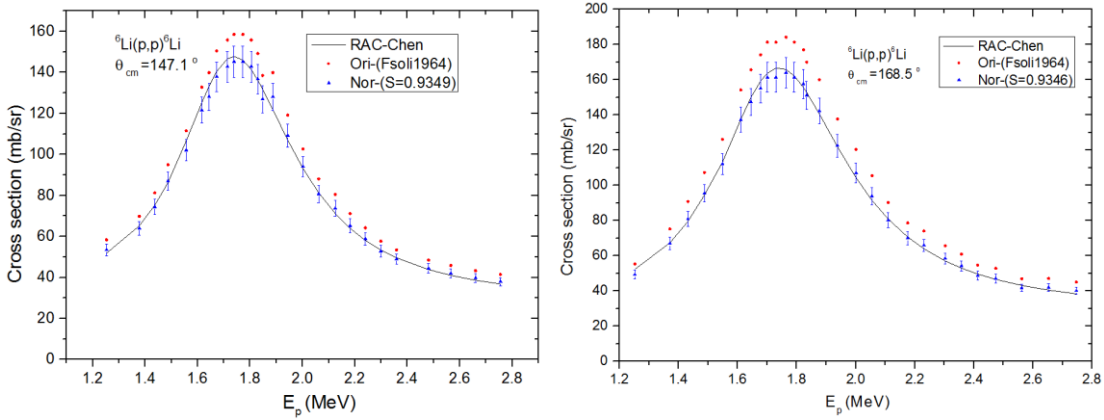


FIG. 3.36. Chen

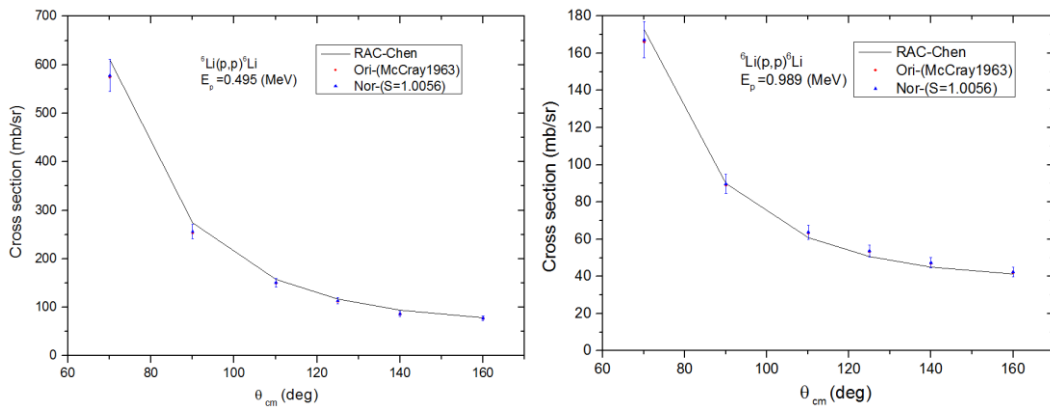


FIG. 3.37. Chen

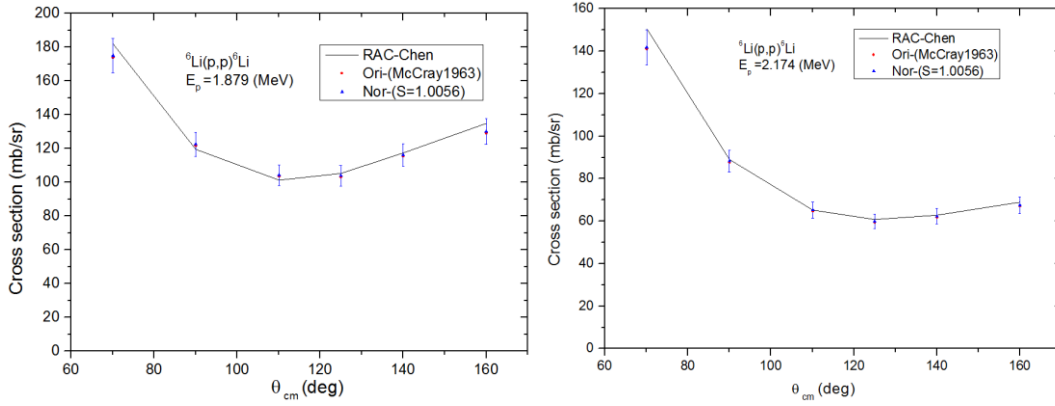


FIG. 3.38. Chen

3.1.4.3. ${}^6\text{Li}(p, {}^4\text{He}) {}^3\text{He}$

In this fit the fitting values of ${}^6\text{Li}(p, {}^4\text{He}) {}^3\text{He}$ depend on ${}^3\text{He}({}^4\text{He}, {}^4\text{He}) {}^3\text{He}$ and ${}^6\text{Li}(p, p) {}^6\text{Li}$. The data of Elwyn1979 and Lin1977 have rather larger system error (about 10%). The Lin1977 has better agreement with the ${}^6\text{Li}(p, {}^4\text{He}) {}^3\text{He}$ and ${}^3\text{He}({}^4\text{He}, {}^4\text{He}) {}^3\text{He}$. In Elwyn1979 the data at 2.277, 2.377 and 2.476 MeV have much low system error (about -20%).

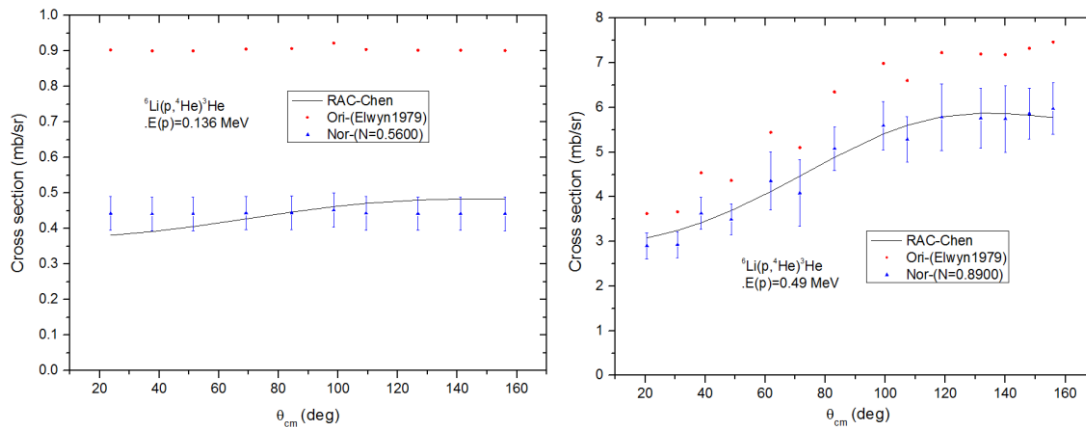


FIG. 3.39. Chen

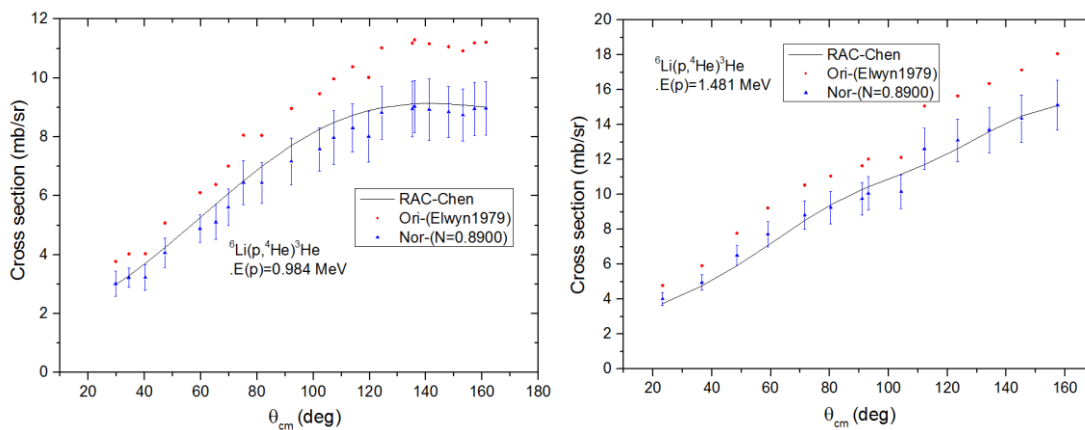


FIG. 3.40. Chen

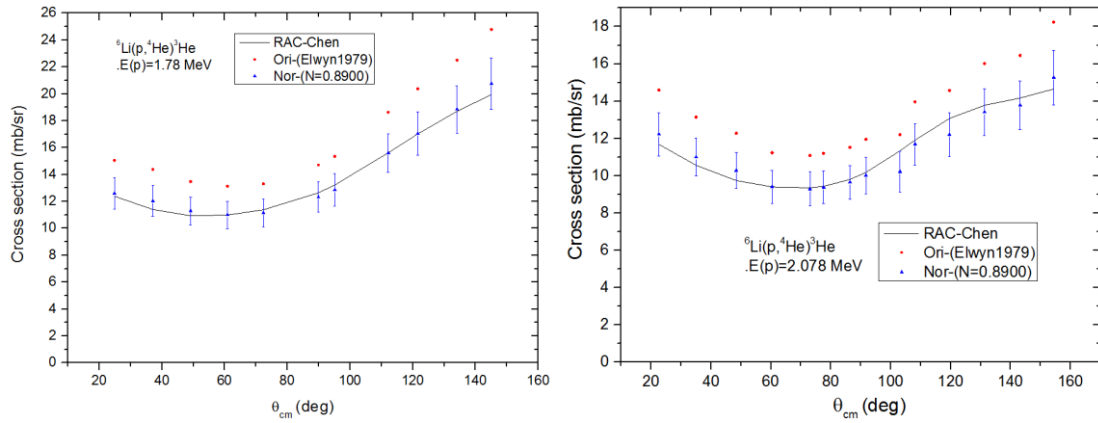


FIG. 3.41. Chen

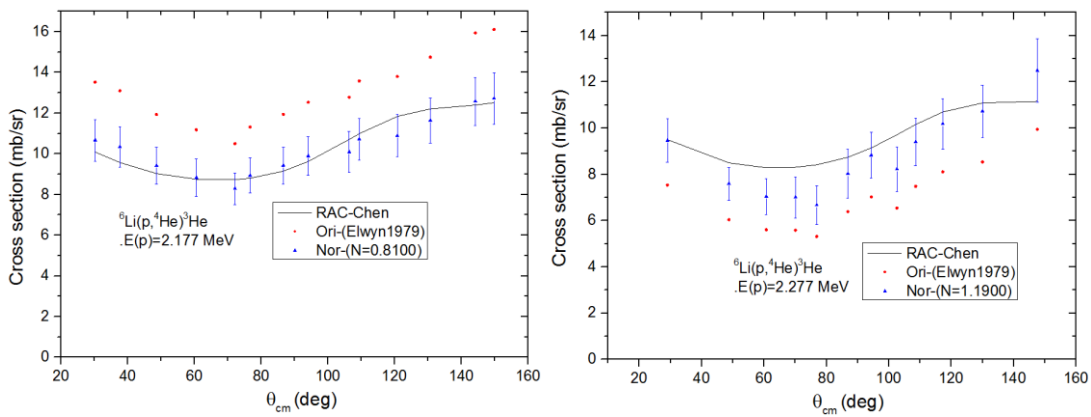


FIG. 3.42. Chen: The data at 2.177 MeV have much high system error (about +20%).

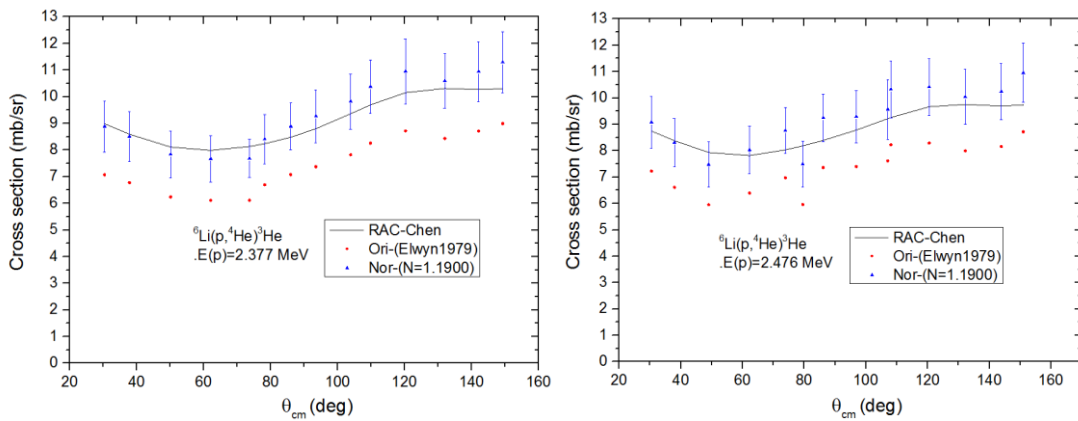


FIG. 3.43. Chen: In Elwyn 1979 the data at 2.277, 2.377 and 2.476 MeV have much low system error (about -20%).

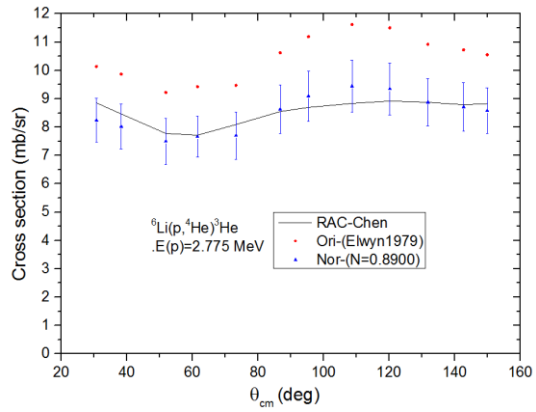
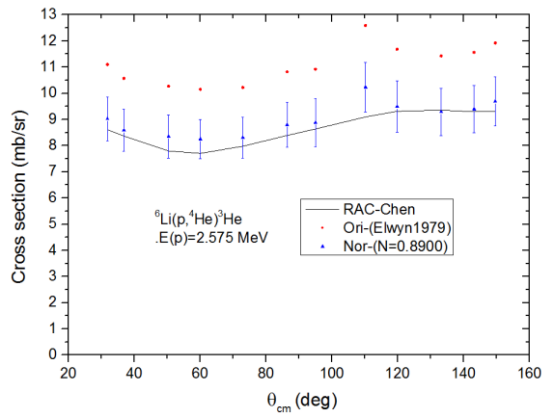


FIG. 3.44. Chen

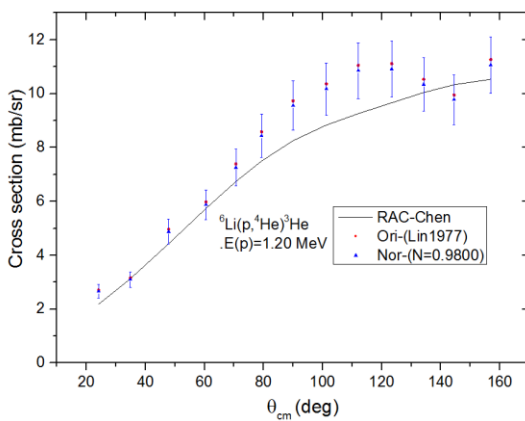
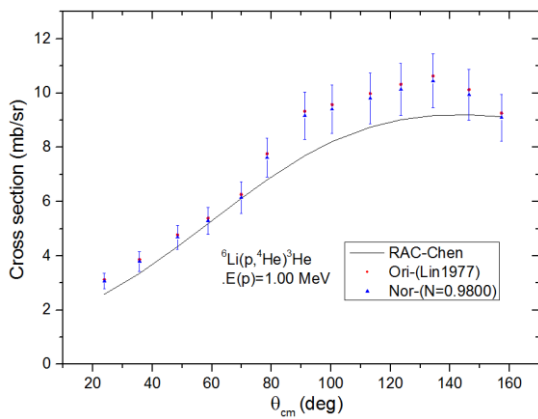


FIG. 3.45. Chen

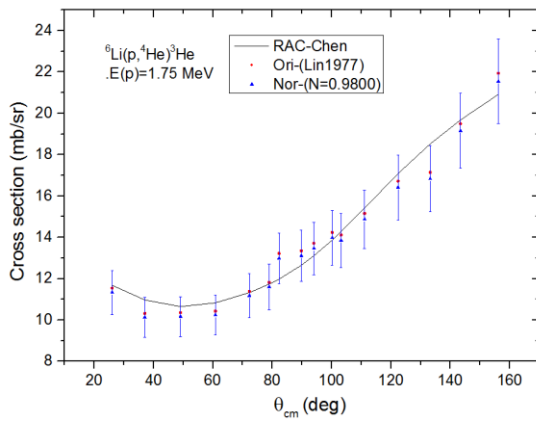
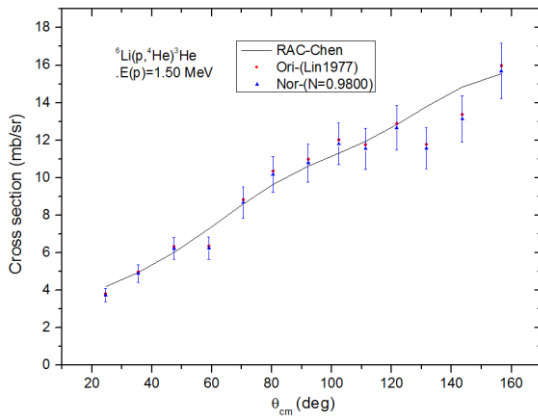


FIG. 3.46. Chen

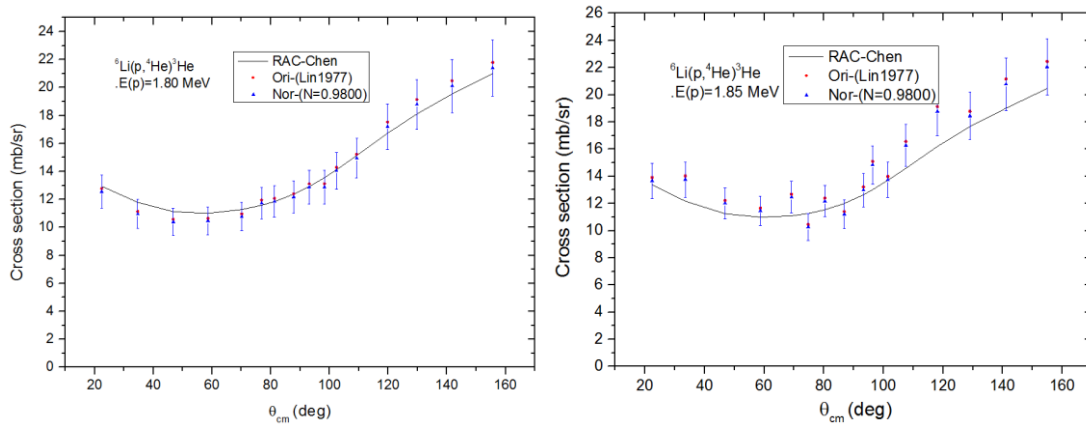


FIG. 3.47. Chen

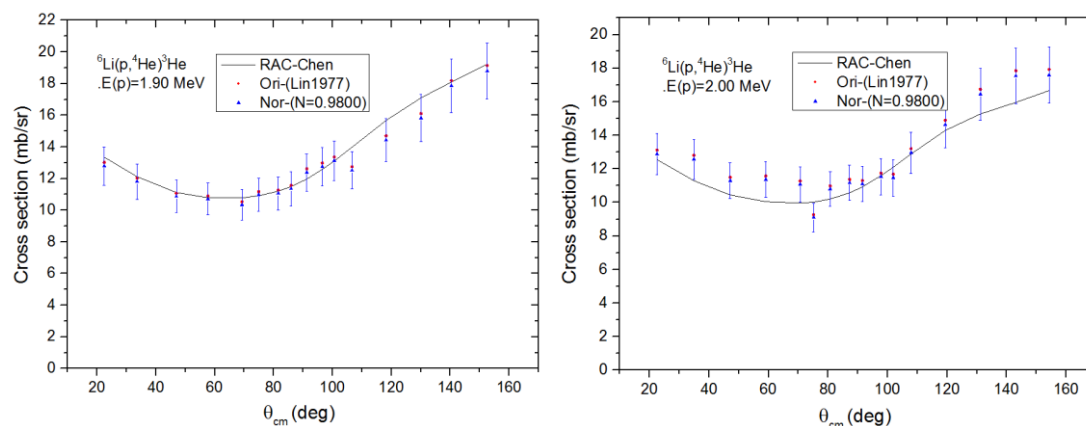


FIG. 3.48. Chen

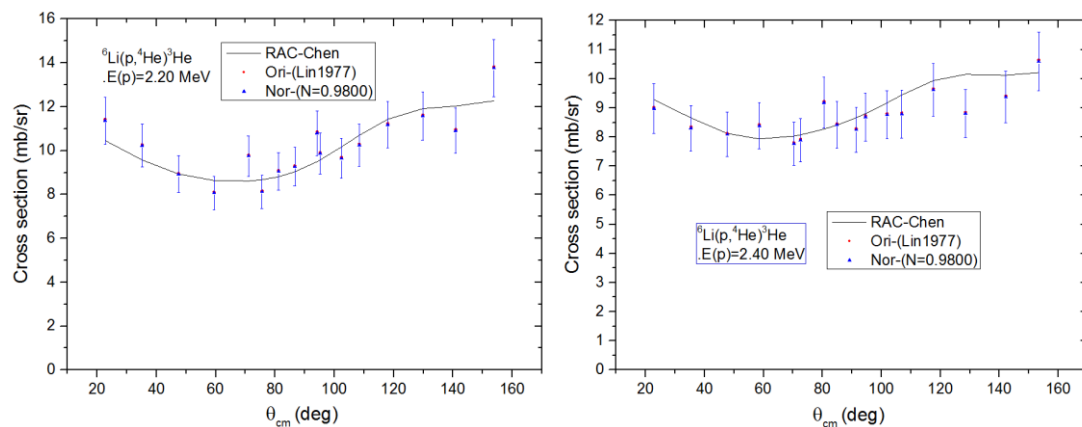


FIG. 3.49. Chen

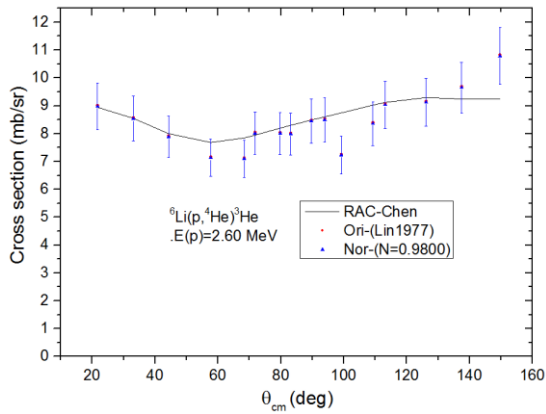


FIG. 3.50. Chen

3.1.4.4. ${}^3\text{He}({}^4\text{He}, p){}^6\text{Li}$

In this fit the fitting values of ${}^3\text{He}({}^4\text{He}, p){}^6\text{Li}$ depend on ${}^3\text{He}({}^4\text{He}, {}^4\text{He}){}^3\text{He}$ and ${}^6\text{Li}(p, p){}^6\text{Li}$.

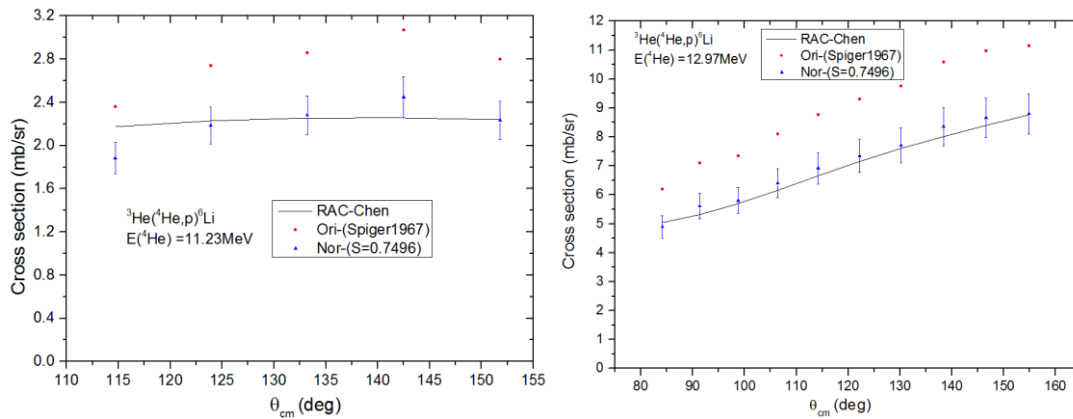


FIG. 3.51. Chen

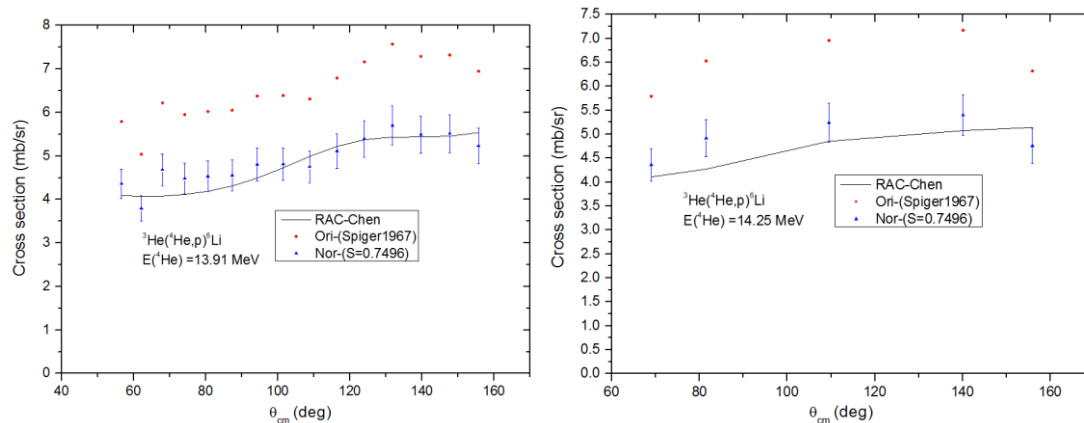


FIG. 3.52. Chen

Discussion:

In these fits, although the normalization factor is kept within the systematic errors mentioned in the papers, the errors on the data are increased when $\chi^2/N > 9$ in order to get a better fit. Chen is kindly asked to provide all the formula he uses to calculate the cross sections using the reduced R-matrix theory.

3.1.5. Test 1b results with SAMMY, M. Pigni, ORNL

The Test 1b using the SAMMY code was performed for two cases. The first case was performed only for the subset of experimental data related to the incident α -particle kinematics. Here, the proton induced experimental data were not included because the SAMMY code does not currently have the capability to include incident particle-pairs for different target nuclei fully integrated in the fitting procedure. For Test 1b, the treatment of different incident particle-pairs was partially included in SAMMY by converting the parameter file from the $\alpha+{}^3\text{He}$ kinematics to the $p+{}^6\text{Li}$ kinematics. However, the conversion from one kinematics to another is not implemented for the covariance matrix of the resonance parameters yet.

To perform the fit of the experimental data for incident α -particle reaction channels listed for the Test 1b, the initial resonance energies used in SAMMY consisted of two bound states related to the ground state and the first excited state of ${}^7\text{Be}$ plus the resonance energies for the 2nd,3rd,4th,5th levels of the same compound nucleus.

Additional poles energies at $E_{\text{alab}} = 46$ MeV for each $J\pi$ were included. The initial values of the reduced-amplitudes were taken from the table of the test case document when possible or set to $100\sim\text{eV}^{1/2}$.

The fit of the experimental data with the SAMMY was performed by a sequential Bayesian update that included several iterations. The initial uncertainty on the reduced amplitudes was set to 50% and a very small uncertainty was set on the resonance energies. The experimental data included in the Bayesian fit did not account for the related experimental covariance matrix. Therefore, the experimental uncertainty used in the fitting procedure was only the statistical one. The average $\chi^2 = 6.6$ for the first case was obtained under these conditions and examples of the fitted data for α -particle induced reactions are shown in the following figures.

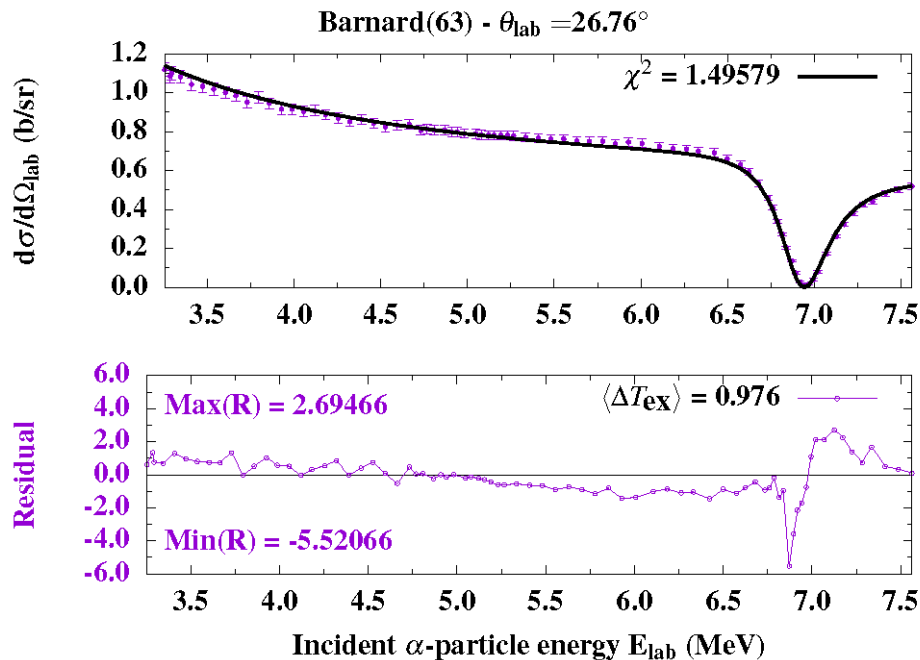


FIG. 3.53. Pigni: Excitation function of ${}^3\text{He}(\alpha,el)$ reaction for $\vartheta_{\text{lab}}=26.76^\circ$. (Top) Comparison of experimental and calculated values. The calculated values are normalized by 1.004. (Bottom) residual defined by the difference of experimental and calculated values weighted by the experimental uncertainty (Case 1).

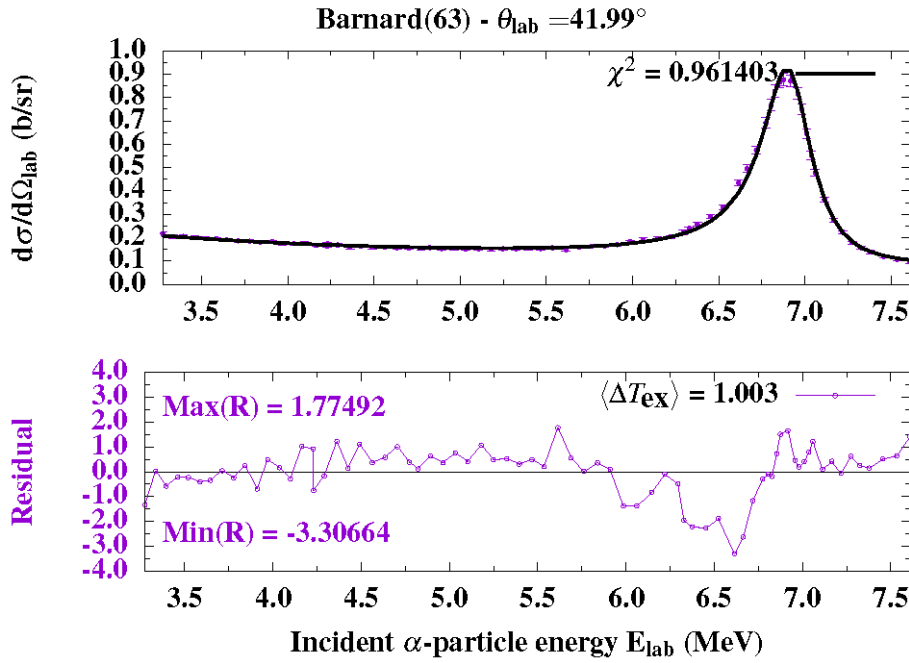


FIG. 3.54. Pigni: Excitation function of $^3\text{He}(\alpha, e\ell)$ reaction for $\vartheta_{\text{lab}}=41.99^\circ$. (Top) Comparison of experimental and calculated values. The calculated values are normalized by 1.004. (Bottom) residual defined by the difference of experimental and calculated values weighted by the experimental uncertainty (Case 1).

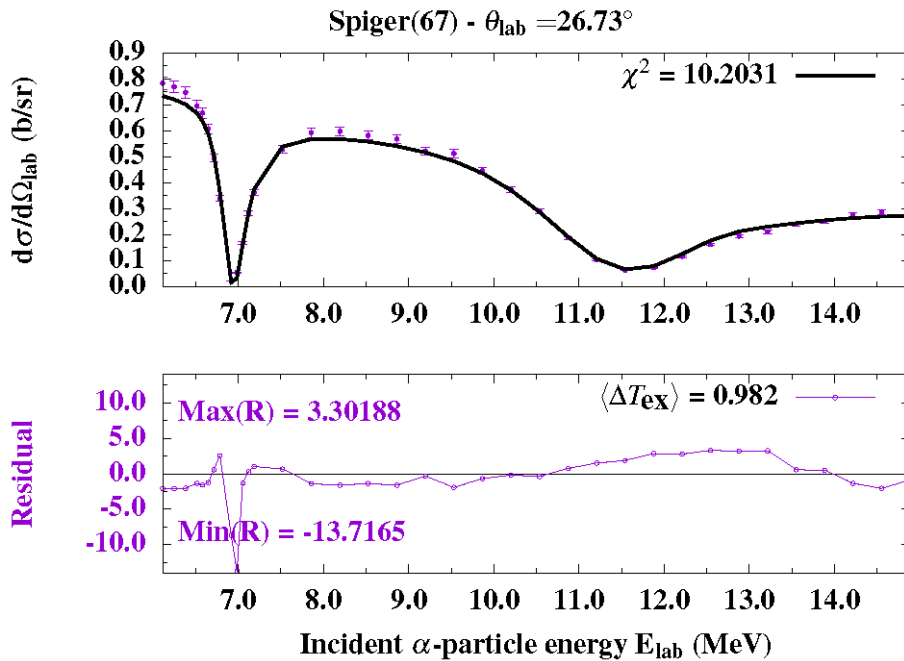


FIG. 3.55. Pigni: Excitation function of $^3\text{He}(\alpha, e\ell)$ reaction for $\vartheta_{\text{lab}}=26.73^\circ$. (Top) Comparison of experimental and calculated values. The calculated values are normalized by 1.078. (Bottom) residual defined by the difference of experimental and calculated values weighted by the experimental uncertainty (Case 1).

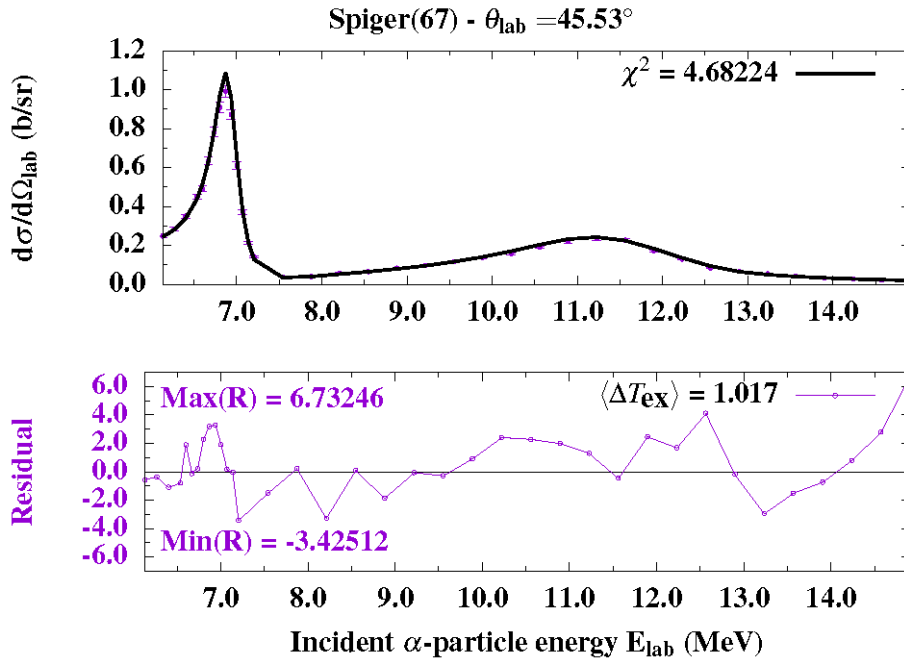


FIG. 3.56: Pigni: Excitation function of ${}^3\text{He}(\alpha, e\ell)$ reaction for $\vartheta_{\text{lab}}=45.53^\circ$. (Top) Comparison of experimental and calculated values. The calculated values are normalized by 1.078. (Bottom) residual defined by the difference of experimental and calculated values weighted by the experimental uncertainty (Case 1).

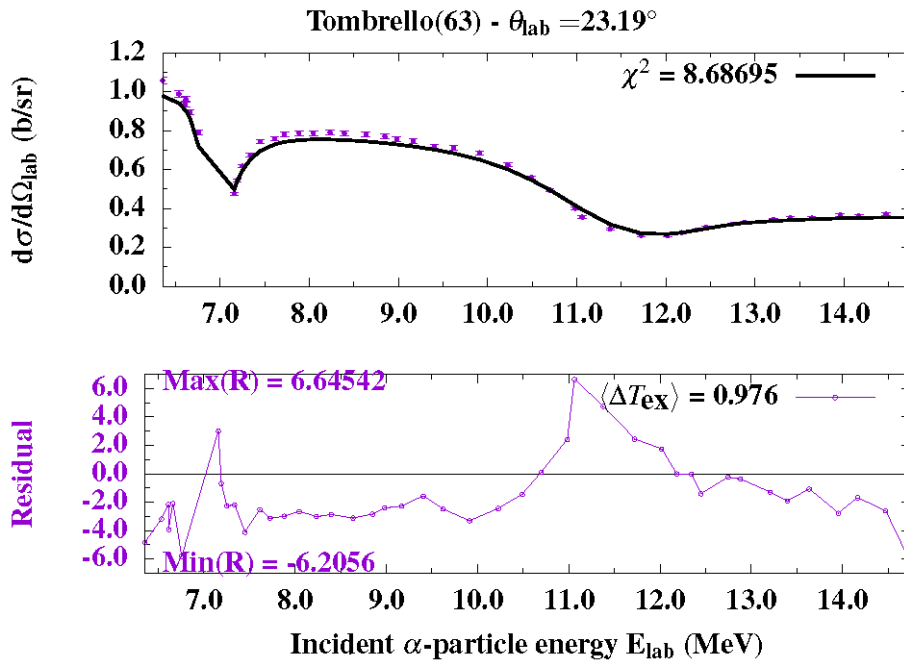


FIG. 3.57: Pigni: Excitation function of ${}^3\text{He}(\alpha, e\ell)$ reaction for $\vartheta_{\text{lab}}=23.19^\circ$. (Top) Comparison of experimental and calculated values. The calculated values are normalized by 0.920. (Bottom) residual defined by the difference of experimental and calculated values weighted by the experimental uncertainty (Case 1).

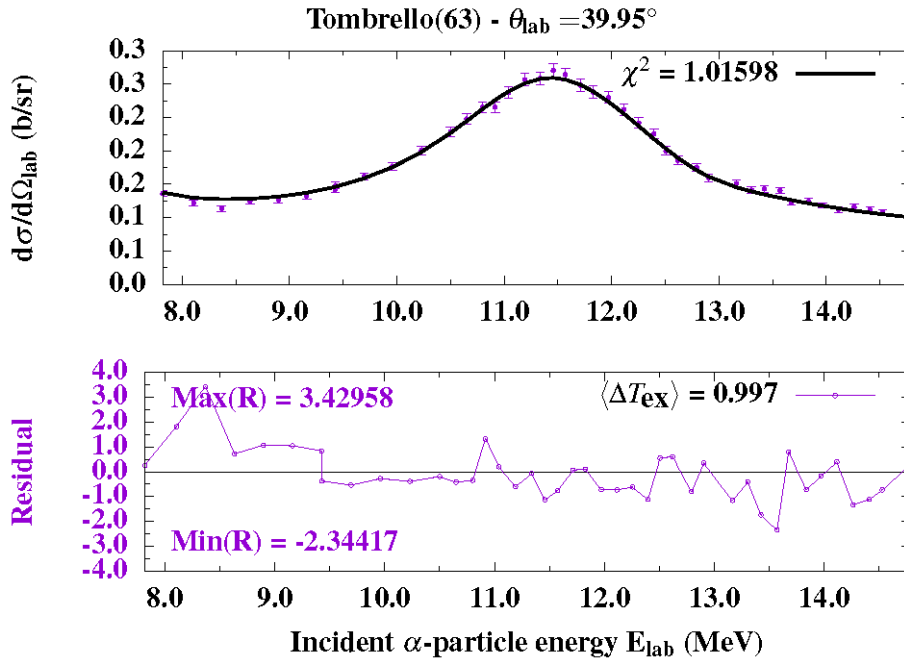


FIG. 3.58. Pigni: Excitation function of ${}^3\text{He}(\alpha,el)$ reaction for $\theta_{lab}=39.95^\circ$. (Top) Comparison of experimental and calculated values. The calculated values are normalized by 0.944. (Bottom) residual defined by the difference of experimental and calculated values weighted by the experimental uncertainty (Case 1).

The second case was produced by using Ian Thompson parameters as a prior information. Here, we used a temporary patch to the SAMMY code to include both partitions, i.e., ${}^4\text{He}+{}^3\text{He}$ and $p+{}^6\text{Li}$, in the Bayesian fitting procedure. The patch consisted of modifying the SAMMY parameter file according to the partition used in the calculations. For the time being, this was not performed for the covariance matrix of the resonance parameters. In this case the prior information accounted for 2 positive parity levels in addition to those ones of the first case.

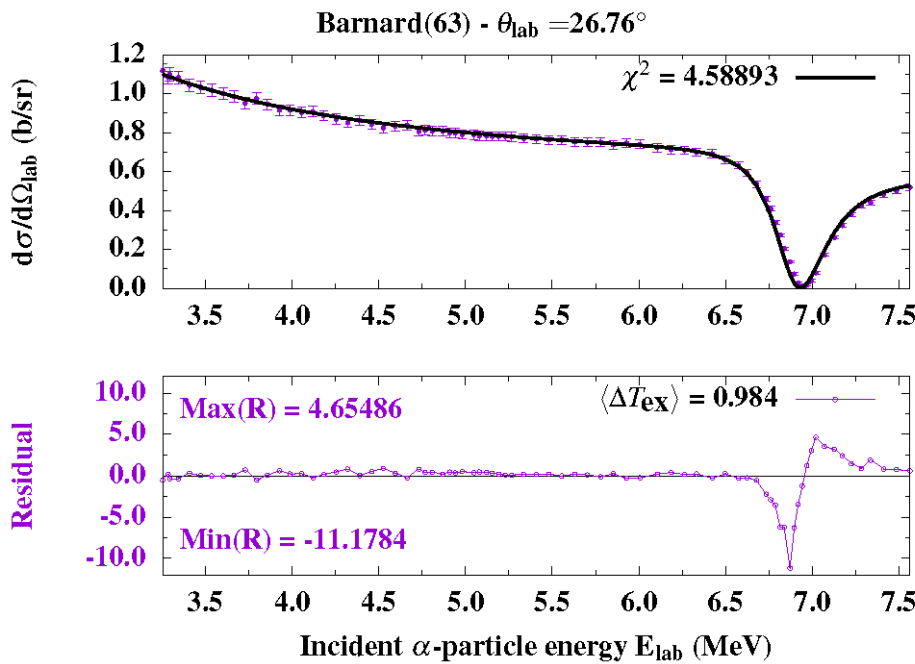


FIG. 3.59. Pigni: Excitation function of ${}^3\text{He}(\alpha,el)$ reaction for $\theta_{lab}=26.76^\circ$. (Top) Comparison of experimental and calculated values. The calculated values are normalized by 1.004. (Bottom) residual defined by the difference of experimental and calculated values weighted by the experimental uncertainty (Case 2).

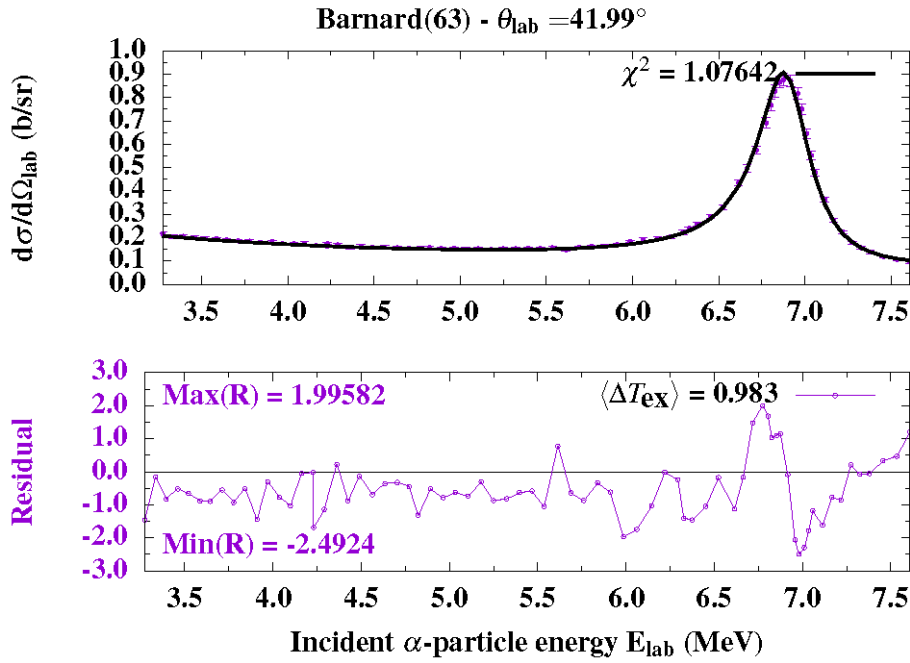


FIG. 3.60. Pigni: Excitation function of ${}^3\text{He}(\alpha, e\ell)$ reaction for $\vartheta_{\text{lab}}=41.99^\circ$. (Top) Comparison of experimental and calculated values. The calculated values are normalized by 1.004. (Bottom) residual defined by the difference of experimental and calculated values weighted by the experimental uncertainty (Case 2).

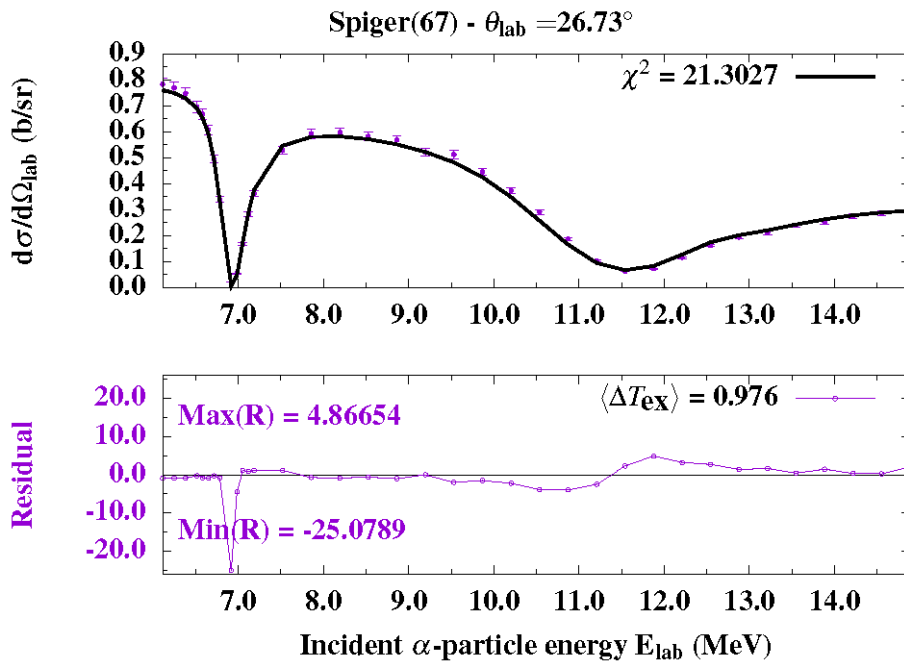


FIG. 3.61. Pigni: Excitation function of ${}^3\text{He}(\alpha, e\ell)$ reaction for $\vartheta_{\text{lab}}=26.73^\circ$. (Top) Comparison of experimental and calculated values. The calculated values are normalized by 1.078. (Bottom) residual defined by the difference of experimental and calculated values weighted by the experimental uncertainty (Case 2).

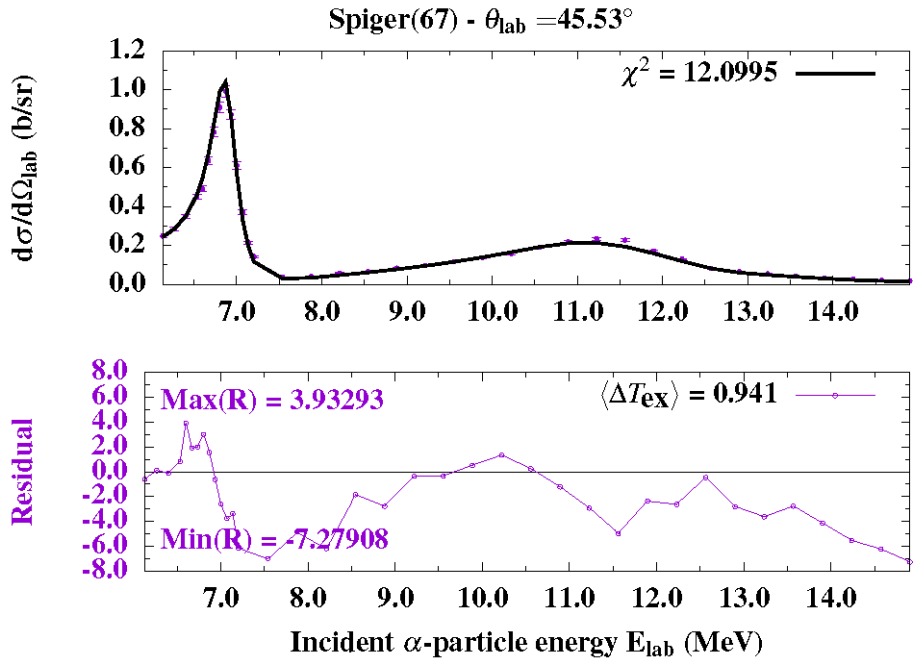


FIG. 3.62. Pigni: Excitation function of ${}^3\text{He}(\alpha,el)$ reaction for $\vartheta_{lab}=45.53^\circ$. (Top) Comparison of experimental and calculated values. The calculated values are normalized by 1.078. (Bottom) residual defined by the difference of experimental and calculated values weighted by the experimental uncertainty (Case 2).

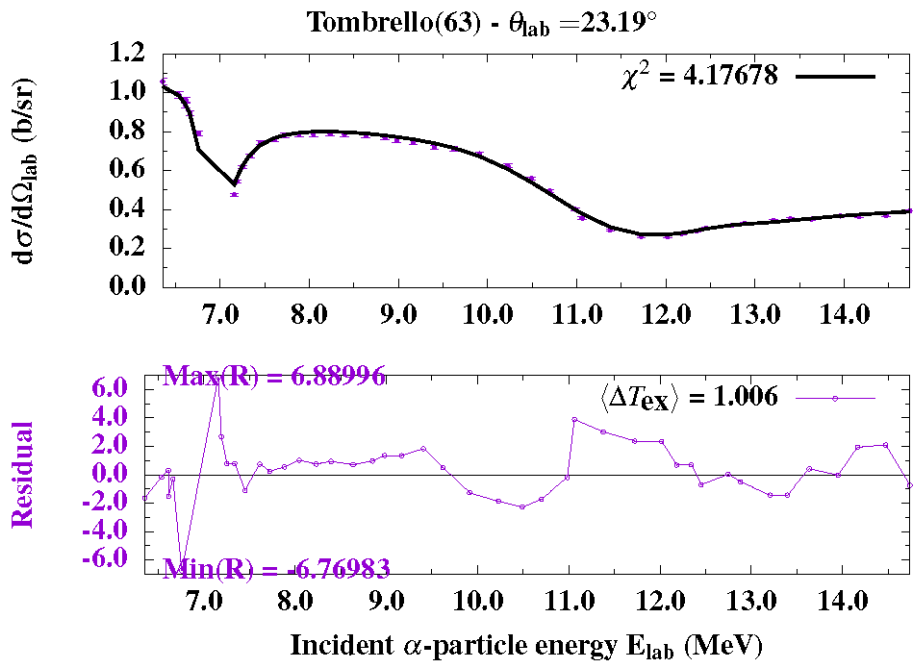


FIG. 3.63. Pigni: Excitation function of ${}^3\text{He}(\alpha,el)$ reaction for $\vartheta_{lab}=23.19^\circ$. (Top) Comparison of experimental and calculated values. The calculated values are normalized by 0.920. (Bottom) residual defined by the difference of experimental and calculated values weighted by the experimental uncertainty (Case 2).

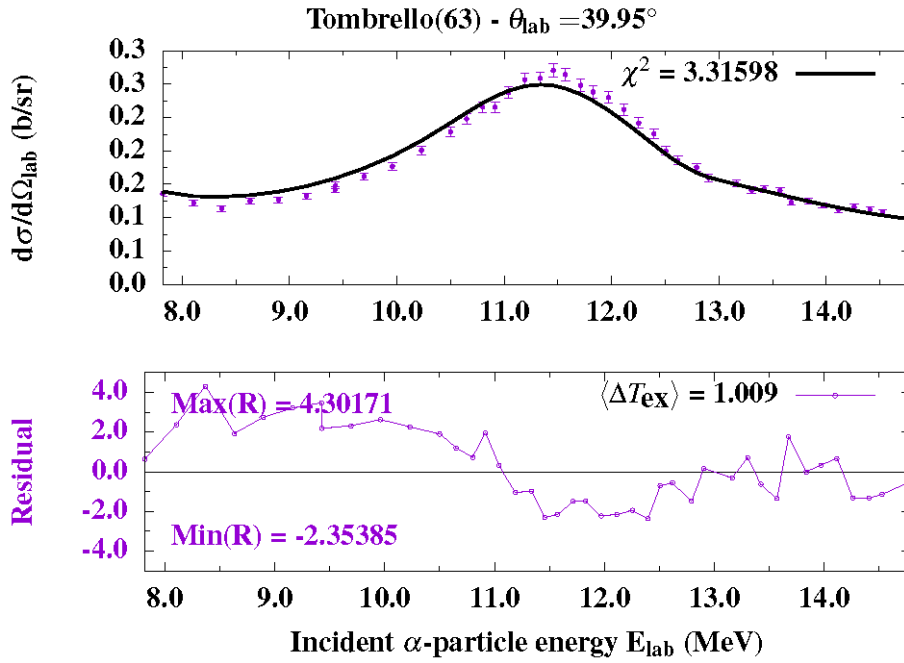


FIG. 3.64. Pigni: Excitation function of ${}^3\text{He}(\alpha,el)$ reaction for $\vartheta_{lab}=39.95^\circ$. (Top) Comparison of experimental and calculated values. The calculated values are normalized by 0.944. (Bottom) residual defined by the difference of experimental and calculated values weighted by the experimental uncertainty (Case 2).

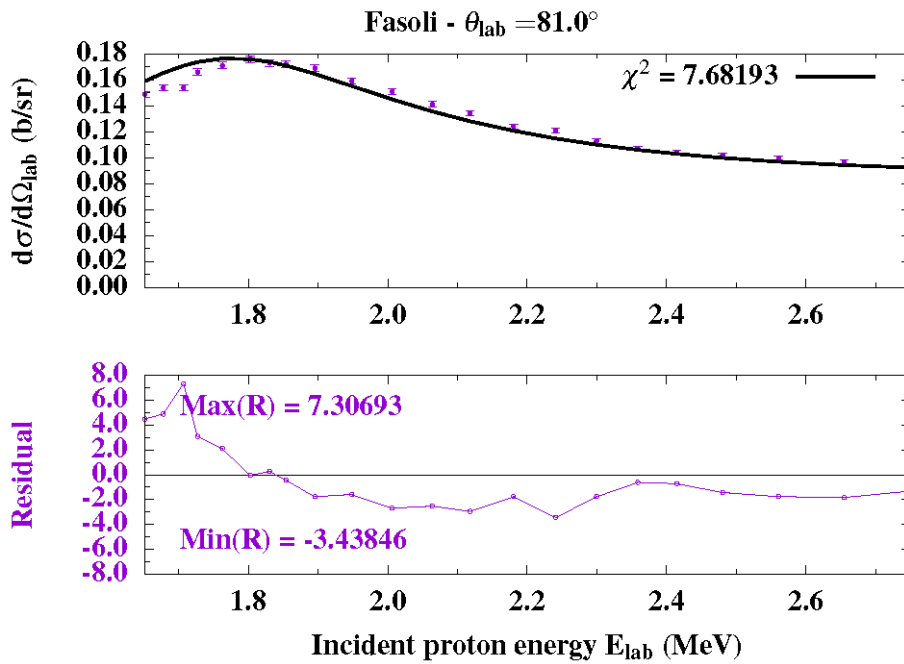


FIG. 3.65. Pigni: Excitation function of ${}^6\text{Li}(p,el)$ reaction for $\vartheta_{lab}=81^\circ$. (Top) Comparison of experimental and calculated values. The calculated values are normalized by 1.198. (Bottom) residual defined by the difference of experimental and calculated values weighted by the experimental uncertainty (Case 2).

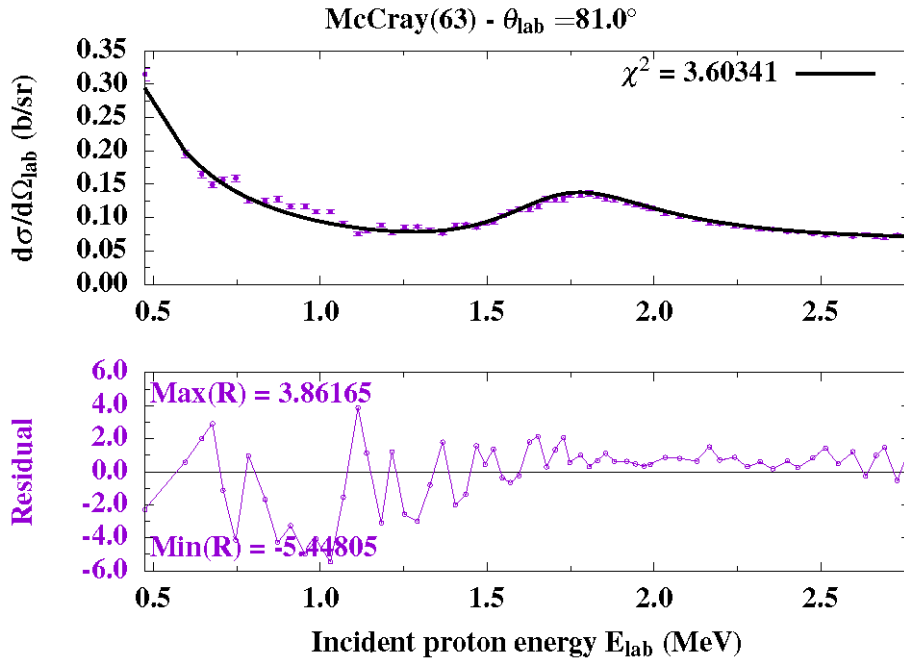


FIG. 3.66. Pigni: Excitation function of ${}^6\text{Li}(p,e)$ reaction for $\vartheta_{\text{lab}}=81.0^\circ$. (Top) Comparison of experimental and calculated values. The calculated values are normalized by 0.935. (Bottom) residual defined by the difference of experimental and calculated values weighted by the experimental uncertainty (Case 2).

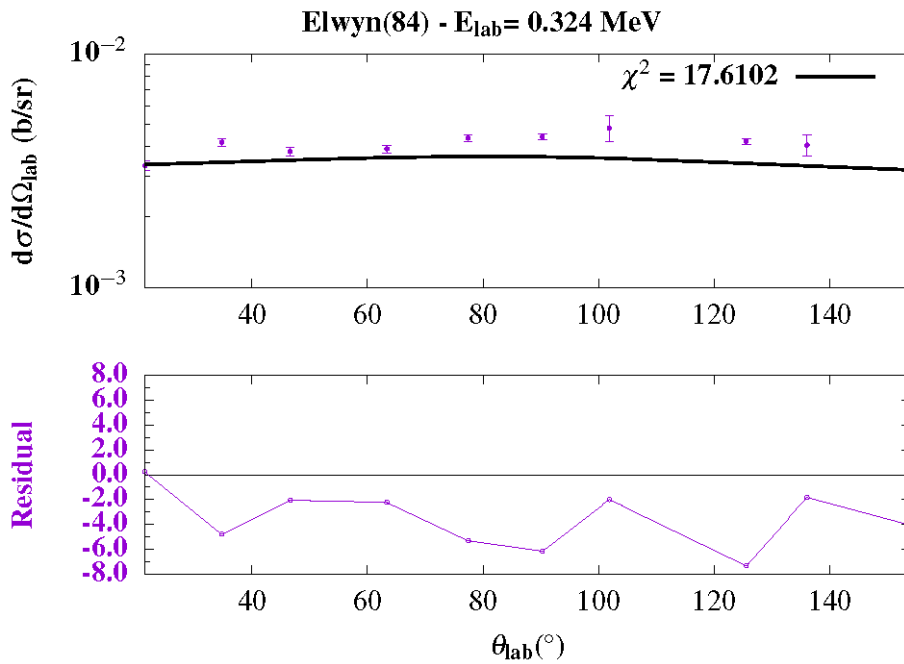


FIG. 3.67. Pigni: Angular distribution of ${}^6\text{Li}(p,\alpha)$ reaction for $E_{\text{lab}}=0.324\sim\text{MeV}$. (Top) Comparison of experimental and calculated values. The calculated values are normalized by 0.879. (Bottom) residual defined by the difference of experimental and calculated values weighted by the experimental uncertainty (Case 2).

TABLE 3.3 Particle Properties. Masses are in amu, and excitation energies in MeV.

Particle	Mass	Charge	Spin	Parity	E*
Be7	7.01863	4	None	None	None
H1	1.0078	1	0.5	1	0.0
He3	3.01603	2	0.5	1	0.0
He4	4.0026	2	0	1	0.0
Li6	6.0151	3	1	1	0.0
photon	0	0	1	1	0.0

TABLE 3.4 Channel Properties. Q values are in MeV, and radii in fm.

GND Label	Projectile	Target	Q value	Radius	Compound	Eliminated
photon + Be7	photon	Be7	0	4.241511	Be7	True
He4 + He3	He4	He3	0	4.241511	Be7	False
H1 + Li6	H1	Li6	-4.01972	3.943969	Be7	False

TABLE 3.5 R-matrix parameters in the B = -L basis. Pole energies in the laboratory frame of the elastic channel ${}^4\text{He} + {}^3\text{He}$. Formal widths Γ_c (in the ENDF6 convention) in units of MeV (lab).

$J\pi = 0.5+$ (zero for all $L \geq 1$)					
E	photon+Be7	He4+He3	H1+Li6		
(MeV)	LS: 0, 0	LS: 0, 1/2	LS: 0, 1/2		
46.534 B	0	139.8257	34.34052		
$J\pi = 0.5$					
E	photon+Be7	He4+He3	H1+Li6	H1+Li6	
(MeV)	LS: 0, 0	LS: 1, 1/2	LS: 1, 1/2	LS: 1, 3/2	
-2.607035	0	-0.29649	1.4677	0	
46.539 B	0	33.36515	-0.2846	0	
$J\pi = 1.5$ (zero for all $L \geq 2$)					
E	photon+Be7	He4+He3	H1+Li6	H1+Li6	
(MeV)	LS: 0, 0	LS: 1, 1/2	LS: 1, 1/2	LS: 1, 3/2	
-3.653163	0	0.33516	14.22882	0.55399	
46.539 B	0	49.70797	-17.91839	0	
$J\pi = 1.5+$					
E	photon+Be7	He4+He3	H1+Li6	H1+Li6	H1+Li6
(MeV)	LS: 0, 0	LS: 2, 1/2	LS: 0, 3/2	LS: 2, 1/2	LS: 2, 3/2
46.537 B	0	88.16119	19.40444	0	0
$J\pi = 2.5+$ (zero for all $L \geq 3$)					
E	photon+Be7	He4+He3	H1+Li6	H1+Li6	
(MeV)	LS: 0, 0	LS: 2, 1/2	LS: 2, 1/2	LS: 2, 3/2	
46.539 B	0	76.10885	0.0694	0	

J π = 2.5					
E	photon+Be7	He4+He3	H1+Li6	H1+Li6	H1+Li6
(MeV)	LS: 0, 0	LS: 3, 1/2	LS: 1, 3/2	LS: 3, 1/2	LS: 3, 3/2
13.83685	0	0.33229	2.16854	0	0
18.454 B	0	-10.79376	0.96677	-0.28896	0.00081
46.541 B	0	18.38693	-42.20427	0	0
J π = 3.5 (zero for all L \geq 4)					
E	photon+Be7	He4+He3	H1+Li6	H1+Li6	
(MeV)	LS: 0, 0	LS: 3, 1/2	LS: 3, 1/2	LS: 3, 3/2	
7.949031	0	0.53797	0	0	
46.540 B	0	-62.73566	14.91057	0	
J π = 3.5+					
E	photon+Be7	He4+He3	H1+Li6	H1+Li6	H1+Li6
(MeV)	LS: 0, 0	LS: 4, 1/2	LS: 2, 3/2	LS: 4, 1/2	LS: 4, 3/2
46.542 B	0	38.26552	1.25579	0	0
J π = 4.5+ (zero for all L \geq 5)					
E	photon+Be7	He4+He3	H1+Li6	H1+Li6	
(MeV)	LS: 0, 0	LS: 4, 1/2	LS: 4, 1/2	LS: 4, 3/2	
46.542 B	0	26.59006	0.02582	0	
J π = 4.5					
E	photon+Be7	He4+He3	H1+Li6	H1+Li6	H1+Li6
(MeV)	LS: 0, 0	LS: 5, 1/2	LS: 3, 3/2	LS: 5, 1/2	LS: 5, 3/2
46.542 B	0	0.03542	0.02574	0	0

3.1.6. ⁷Be analysis with EDA, G. Hale, LANL

The R-matrix analyses that have been done at LANL on reactions in the ⁷Be system was presented. The parameters of the analyses did not follow the form of the Test 1b exercise, but an attempt was made to include the same cross section data as the other participants had used. The analyses were done in several forms, as summarized in the table below. χ^2

TABLE 3.6 Different forms of R-matrix analysis of the ⁷Be system.

Solution	# data pts.	χ^2/dof	Content	Comment
Soln 1 (base)	2292	1.90	Most cross sections + pols.	Started in 1975
Soln2	2780	2.65	Added Mohr, Elwin, Lin	Data questionable
Soln3	3165	4.22	Added Tombrello & Parker	Data not recommended
Soln4	2609	1.20	From Soln2 with $\chi^2_{\text{max}} = 10$	Best parameters?

The first one is a base-line solution that included most of the cross-section data and has a chi-squared per degree of freedom of 1.9. In the second solution, the ³He+⁴He elastic scattering data of Mohr [1] were added, as well as the ⁶Li(p, α)³He differential cross section of Elwyn [2] and of Lin [3], to give a chi-squared per degree of freedom of 2.65. A third solution added the ³He(α , α)³He scattering data of Tombrello and Parker [4], and the chi-squared per degree of freedom increased to 4.22. A fourth solution was started from the second one, with the condition that all data points having chi-squared > 10 were eliminated from the data set. This solution achieved a reasonable chi-squared per degree of freedom of 1.20.

The following conclusions were drawn about the experimental data from these analyses: The Tombrello and Parker [4] data are inconsistent with a later measurement by Spiger and Tombrello [5]. The results of Solution 3 confirmed what we had been told years ago by the Rice University experimentalists who had constructed most of our data set from the original sources, that the Spiger and Tombrello data [5] supersede the earlier measurement of Tombrello and Parker [4], and should be used in place of them. We also learned from Solution 4 that the added data from Mohr [1], Elwyn [2], and Lin [3] are suspect within their original experimental errors, since many of them were thrown out to achieve the lower value of chi-squared per degree of freedom (1.2).

Our R-matrix parameterization (which included 37 free parameters) was somewhat more flexible than that of Test 1b, which is probably the reason that lower chi-squared values were obtained than in most of the other analyses that maintained the original error bars on the data. The LANL analyses allowed higher-lying positive-energy background levels, and also distant negative-energy levels in addition to the bound states. The physical interpretation of these negative-energy levels is not clear, but they could be connected to the deuteron-exchange mechanism that was proposed by Weigmann [6] in connection with the $1/v$ cross section in the mirror $A = 7$ system for the reaction ${}^6\text{Li}(n,t){}^4\text{He}$.

The resonance parameters for Solution 2, obtained from the complex poles of the S -matrix in the complex E -plane, showed that both the bound $3/2^-$ and $1/2^-$ levels were in the correct positions because of the choice $B = S(E_b)$ in those matrices. Also, the positions and widths of the $7/2^-$ and two $5/2^-$ resonances were in good agreement with the expected values. There was even fair agreement with the position and width of a broad, higher-lying $3/2^-$ resonance that evidently came from detecting the tail of this resonance in the energy range of the data analyzed. There was also a narrow $3/2^+$ resonance found at about 2.5 MeV excitation energy that is probably spurious since there is little or no evidence of it in the experimental data analyzed.

References

- [1] P. Mohr, ${}^3\text{He}+{}^4\text{He}$ elastic scattering at low energies, Phys. Rev. C **48**, 1420 (1993).
- [2] A. J. Elwyn, ${}^6\text{Li}(p,a)$ differential cross sections, Phys. Rev. C **20**, 1984 (1979).
- [3] Lin et al., ${}^6\text{Li}(p,a)$ differential cross sections, Nucl. Phys. A **275**, 93 (1977).
- [4] T.A. Tombrello and P. Parker, Phys. Rev. **130**, 1112 (1963).
- [5] Spiger and T. Tombrello, Phys. Rev. **163**, 964 (1967).
- [6] H. Weigmann and P. Manakos, "Deuteron Exchange Mechanism for the ${}^6\text{Li}(n,\alpha\lambda\pi\eta\alpha)$ Reaction at Low Energies," Z. Phys. A **289**, 383-389 (1979).

Discussions: Hale has used the data of Ivanovich (EXFOR A1014010) which were not included in the Test 1b database from the very beginning. There is an energy shift of Spiger and Tombrello data of about 10keV. He comments that the Test 1b parametrization is probably too limited. Bound states are not in correct positions; more flexible backgrounds are needed. The negative pole is t -variable pole and not an s -variable pole and is not included in R-matrix theory (simulating e.g. d -exchange mechanism). He advises not to use the Tombrello and Parker data of 1963.

3.2. Discussion of Test 1b

- how to constrain bound state energies:

Thompson introduced an additional experimental constraint using a Brune transformation and the corresponding error was then added to the chi2. GH has an alternative method: set boundary condition at $B = S(E_{\text{bound}})$ instead of $B = -L$. Pigni constrained the search around the bound state energy.

- low-lying excited state with $J\pi = 1/2^-$:

Everybody has included it except for Kunieda who omitted it because of the small sensitivity.

- additional poles to those of table 1 (deBoer write-up of Test 1a in [INDC\(NDS\)-0737](#)) were used by some which had a significant impact on the results:

Thompson added broad 3/2+, 5/2+ resonances guided by potential model calculations for the ⁷Be ground state which showed two broad resonances 3/2+ and 5/2+. He obtained this result after having adjusted the potential by 5% to get the bound state. However, it remains to be seen whether these states are needed when doing an evaluation up to higher energies in Test 3.

Chen added many more poles in his Reduced R-matrix approach (28 in total compared to at most 15 used by the others) in order to get the best fit.

Kunieda has added independent distant (background) poles in addition to the background poles of Test 1b. So, for each partition there is an independent background pole for each JT at 20 MeV energy.

Thompson showed the impact of removing the d waves from his fit: strongest impact was on the (p,p)- channel, where the χ^2 is considerably worse. The alpha-channel is not affected that much. D-wave poles have strong coupling to the proton channel. An attempt to refit the data without d-wave poles gave a $\chi^2 = 8.7$.

- Correlations of background poles:

The resonance parameter covariance matrix indicated high correlations among the parameters of the background poles which did not allow for reasonable solutions to be obtained. These strong correlations indicate that the data are not sensitive to the parameters of the set of background poles used. Additional experimental data may yield constraints reducing the correlations between the background poles. Thompson found that fixing the energies and reduced width amplitudes of some of these poles was necessary to solve the problem.

Thompson suggested that looking at the phase shifts on a fine energy grid or looking at the Brune resonance energies helps to spot if unwanted poles have crept in or if bound states have turned into resonances.

- inconsistencies between data sets:
 - o Tombrello and Parker are shifted in energy with respect to the Spiger data (PhD thesis which is now in EXFOR (A1094001)).
 - o there is an energy shift of 0.1 MeV between the Barnard and Spiger data: Barnard original EXFOR entry had problems (due to digitization) as they did not agree at E and angles. They were then digitized by deBoer and sent to the group. But Hale claims that his Barnard and Spiger data are consistent. However, his Barnard data are most probably from the original source.

It is therefore important to compare these data sets and decide which ones should be used in Test 3.

- normalization issues:
 - o Kunieda had to relax the normalization constraints for the different data sets to get an improved χ^2 . His normalization is included in the correlation parameters.
- When scaling the cross sections by normalization factor, the errors should also be scaled but the relative errors should remain unchanged.

- The χ^2 formula by Chen is not the same as the formula used by the rest of the group (include formulas to make things clear).

4. Test 2

In the IAEA Neutron Standards project, the minimization techniques were compared, i.e. how the codes reach the local minimum from a given starting point. This test is more limited in scope than Test 1b but is also useful to test how the different codes perform this basic function so an additional test will be performed by the group, as Test 2, after the paper on Test 1a has been prepared.

Specifications of Test 2:

A consistent set of experimental data needs to be selected, including one data set for each channel ((α,α), (p,p), (α,p) and (p, α)). In addition, the starting input parameters will be defined carefully so that convergence to a fully concave-upward minimum is possible. The minima as well as the covariance matrices will be compared. The covariance matrix should also contain the normalisations.

The bound channels will be fixed following Hale's prescription, i.e. using boundary condition for bound state $B = S(E_{\text{bound}})$ and for all others $B = -L$. The matching radii should be the same as in Test 1a.

Action on Hale and DeBoer: to select the experimental database and determine the starting parameters of the fit.

Deadline 1st February 2019.

Action on all: Perform the fit varying the parameters in the sent input file and send the results to Hale and DeBoer.

Deadline 1st March 2019.

5. Test 3

The objective of Test3 is the evaluation of the ^7Be compound system.

The aim is to go to as high energies as possible.

The proposal is to include the first two proton inelastic channels and also photon channels, i.e. go up to $E_x = 10$ MeV.

The $pd\alpha$ -channel is the first breakup channel at about $E_x \sim 7.0$ MeV. However, it is not yet clear how to include it.

Experimental database:

EXFOR should be searched for all additional data. Chen's database should also be cross-checked for errors. All the original uncertainties in the data are to be used without scaling and the systematic errors are to be treated as 1σ parameters of a Gaussian distribution. The splitting of normalization factors will be decided and recommended in advance.

Action on deBoer and rest of group: to recommend the required splitting of normalization factors for the additional data to be used.

Kinematics:

They should be adopted from original papers compiled in EXFOR. If errors are found in EXFOR entries they should be reported directly to the IAEA (N. Otuka).

The experimental data should be cross-checked with those of Hale to make sure they are complete and correct.

Conditions of Test 3:

- Channels: all channels used in Test 1b including first two inelastic proton channels and photon channels
- Energy range: $E_x < 10$ MeV - still to be decided OR go to as high E_x as data allow
- Data sets: all data must be collected and checked
- Resonance parameters: no constraints except for bound poles agreeing with observed b.s. energies in the Brune basis
- Background poles: no constraints
- Normalization: splitting of normalization functions will follow recommendation

Polarization observables can be included in the fit if the code can calculate them, otherwise they will be calculated with final parameters and compared to data.

Action on all: Complete Test 3 and send results to Thompson.

Deadline: 1st May 2019

The next meeting will be held once the participants have provided results of Test 3 for comparison and discussion.

Finally, Thompson proposed to create a repository in Github with sub-directories for each code where resonance input files and results, figures can be stored and shared widely. The proposal was endorsed. An organization "R-Matrix Analysis of Charged Particle Reactions (RMACPR)" was created at <https://github.com/RMACPR>, and the project repository "Be7 Rmatrix Analysis" was created at https://github.com/RMACPR/Be7_Rmatrix_Analysis.

6. Conclusions and Recommendations

The project results are as follows:

The R-matrix codes were improved, corrected or further improved: never before such an understanding of how the codes work has been achieved, nor such a level of agreement (to 0.1%)

The development of the Ferdinand program has enabled translating between different parameterizations and approximations and understanding the physics behind the R-matrix approach as well as facilitated communication between different code developers and users.

The meeting participants recommend that this group continues the effort to exchange technical expertise and ideas on the development of R-matrix codes, evaluation methodologies and how to implement them to deliver evaluated data ready for dissemination and use in applications.

7. List of Actions

Item #	Action	Responsible	Deadline
1	Provide the values of fundamental constants and atomic masses consistent with the empirical Q-values used in Test 1a.	DeBoer	29 Aug. 2018 (Completed)
2	Coordinate the comparison of Coulomb functions (energy shift S , penetrability P and the hard sphere phase shift ϕ).	Thompson	29 Aug. 2018 (Completed)
3	Prepare requested files with S , P and ϕ and send them to Thompson for comparison.	All participants of R-matrix group	15 Sept. 2018
4	Provide final Test 1a cross sections for all channels to DeBoer.	All participants of R-matrix group	15 Oct. 2018
5	complete the first draft of the paper and share it with the group on Overleaf.	Dimitriou	3 Sept. 2018 (Completed)
6	Monitor the preparation of the paper, contact EPJ A about submission, probable date, volume etc.	Dimitriou	30 Sept. 2018.
7	Prepare final draft of the paper for submission	All participants of R-matrix group	15 Dec. 2018.
8	Decide on the experimental database to be used in Test 2 and prepare the starting parameter file for the fit.	Hale and DeBoer	1st Feb. 2019
9	Perform the fit for Test 2 starting from the parameters in the sent input file (#x) and send the results to Hale and DeBoer.	All participants of R-matrix group	1st March 2019
10	Recommend the splitting of normalization factors per excitation function or angular distributions for the additional data to be used in Test 3.	DeBoer with contribution from all participants of R-matrix group	After Test 2 is completed – 1st May 2019
11	Complete Test 3 and send results to Thompson.	All participants	1 May 2019



Consultants' Meeting on
**“R-matrix Codes for Charged-particle Reactions
in the Resolved Resonance Region”**

IAEA, Vienna, Austria
27 to 29 August 2018
Meeting Room VIC MOE15

PRELIMINARY AGENDA

Monday, 27 August

- 08:30 – 09:00** **Registration (IAEA Registration Desk, Gate 1)**
- 09:00 – 09:30** **Opening Session**
Welcoming address (Arjan Koning, NDS Section Head)
Administrative matters
Election of Chairman and Rapporteur
Adoption of the Agenda
- 09:30 – 17:30** **Presentations by participants on Test1b results (~ 40 min each)**
- 1) Results of Test1a, R. DeBoer (Univ. Notre Dame)
 - 2) Test1b results with SFRESCO, I. Thompson (LLNL)
 - 3) Test1b results with AZURE, R. DeBoer (Univ. Notre Dame)
 - 4) Test1b results with AMUR, S. Kunieda (JAEA)
 - 5) Test1b results with RAC, Z. Chen (Tsinghua Univ.)
 - 6) Test1b results with SAMMY, M. Pigni (ORNL)
 - 7) Test1b results with CECCCO, T. Srdinko (TUV)
 - 8) ⁷Be analysis with EDA, G. Hale (LANL)
 - 9) P. Dimitriou (IAEA)

Coffee break(s) as needed

(12:30 – 14:00 Lunch break)

Tuesday, 28 August

09:00 – 17:30 Round Table Discussions

- Results of Test1b – how do we proceed with evaluation project
- Inter-changeability of R-matrix parameters with Ferdinand: can we replicate all codes' results with the provided resonance parameters?
- Evaluation methodology:
 - o Experimental data covariances
 - o Preservation of data norms with evaluations
 - o Angular distributions of decay gammas: including them in the fit
 - o Unobserved secondary gamma-ray angular distribution work with AZURE2
- Processing codes – ENDF6 format:
 - o Pointwise reconstructions: methods and codes for charged particles
- Covariance matrices:
 - o changes with parameter transformations (e.g. Brune or Barker or formal-rwa),
 - o use of data – parameter covariances from fits
 - o reconstruction of point-data covariances
 - o stochastic instances for modeling
- Drafting of final article
- Other items that can be shared with INDEN meeting:
 - o Plans for new fits of nuclear reaction: Data assessments, data error checking, use of previous fits, etc.
 - o Going above dissociation thresholds: is there a general method?
 - o Can we extend R-matrix theory to higher energies by any simple & well-defined method?
 - o Analysis of the ${}^3\text{He}(a,g){}^7\text{Be}$ data with AZURE2
 - o ${}^{27}\text{Al}+p$ work done with AZURE2
 - o How ${}^{12}\text{C}(p,p)$ and ${}^{12}\text{C}(a,a)$ scattering would be extremely useful as charged particle standard reactions, similar to the way ${}^{12}\text{C}(n,n)$ is a neutron standard.

Coffee break(s) as needed

(12:30 – 14:00 Lunch break)

Wednesday, 29 August

09:00 – 17:00 Round Table Discussions cont'd Drafting of the Summary Report Closing of the Meeting

Coffee break(s) as needed

(12:30 – 14:00 Lunch break)

**Consultancy Meeting on
R-Matrix Codes for Charged-particle Reactions in the
Resolved Resonance Region**

27 to 29 August 2018
IAEA, Vienna

List of Participants

AUSTRIA

Helmut **LEEB**
Technical University of Vienna
Atomic Institute
Wiedner Hauptstrasse 8-10
1040 Vienna
E-mail: leeb@kph.tuwien.ac.at

Thomas **SRDINKO**
Technical University of Vienna
Atomic Institute
Wiedner Hauptstrasse 8-10
1040 Vienna
E-mail: tsrdinko@ati.ac.at

CHINA

Zhenpeng **CHEN**
Tsinghua University
100084 Beijing
E-mail: zhpchen@tsinghua.edu.cn

FRANCE

Pascal **ARCHIER**
Batiment 230
Centre d'Etudes Nucleaires de Cadarache
13108 Saint-Paul-lez-Durance
E-mail: pascal.archier@cea.fr

JAPAN

Satoshi **KUNIEDA**
Japan Atomic Energy Agency
Nuclear Data Center
2-4 Shirakata Shirane, Naka-gun
Tokai 319-1195
E-mail: kunieda.satoschi@jaea.go.jp

USA

Gerald **HALE**
Los Alamos National Laboratory
PO Box 1663
Los Alamos NM 87545
E-mail: ghale@lanl.gov

Marco **IGNI**
Oak Ridge National Laboratory
P.O. Box 2008, Bldg 5700
Oak Ridge TN37831
E-mail: pignimt@ornl.gov

Ian **THOMPSON**
Lawrence Livermore National Laboratory
P.O. Box 808, L-414,
Livermore CA 94551
E-mail: thompson97@llnl.gov

Richard J. **DEBOER**
225 Nieuwland Science Hall
Notre Dame IN 46556
E-mail: richard.j.deboer.12@nd.edu

EC-JRC

Stefan **KOPECKY**
European Commission, Joint Research Centre
Directorate G, Nuclear Safety and Security
Retiesweg 11
2440 Geel
E-mail: stefan.kopecky@ec.europa.eu

IAEA

Paraskevi (Vivian) **DIMITRIOU**
Tel. +43-1-2600 21708
E-mail: p.dimitriou@iaea.org

Arjan **KONING**
E-mail: a.koning@iaea.org

Andrej **TRKOV**
E-mail: a.trkov@iaea.org

All:
IAEA/NAPC/Nuclear Data Section
Wagramer Strasse 5
1400 Vienna
Austria

Annex 3

Participants' Presentations

#	Author	Title	Link
1	R.J. deBoer	Test1a + Test1b	PDF
2	I.J. Thompson	R-matrix evaluation of ^7Be system using Fresco and Ferdinand methods	PDF
3	Z. Chen	The report for Test1b-10JP-28L ($\chi=0.81$)	PDF
4	S. Kunieda	Test1b analysis for the ^7Be system with the AMUR code	PDF
5	M.T. Pigni	R-matrix analysis on the ^7Be compound nucleus system with the SAMMY code	PDF
6	G. Hale	Test1b	PDF

Nuclear Data Section
International Atomic Energy Agency
Vienna International Centre, P.O. Box 100
A-1400 Vienna, Austria

E-mail: nds.contact-point@iaea.org
Fax: (43-1) 26007
Telephone: (43-1) 2600 21725
Web: <http://nds.iaea.org>
